The impact of purifying and background selection on the inference of population history: problems and prospects

Parul Johri[*, ‡], Kellen Riall[*], Hannes Becher[†], Brian Charlesworth[†], and Jeffrey D. Jensen[*, ‡]

[*]School of Life Sciences, Arizona State University, Tempe, AZ 85287, USA

[†]Institute of Evolutionary Biology, School of Biological Sciences, University of Edinburgh, EH9 3FL, United Kingdom

[‡]Correspondence can be addressed to these authors

Corresponding authors:

Parul Johri

pjohri1@asu.edu

Jeffrey D. Jensen

Jeffrey.D.Jensen@asu.edu

ABSTRACT

Current procedures for inferring population history are generally performed under the assumption of complete neutrality - that is, by neglecting both direct selection and the effects of selection on linked sites. We here examine how the presence of direct purifying and background selection may bias demographic inference by evaluating two commonly-used methods (MSMC and *fastsimcoal2*), specifically studying how the underlying shape of the distribution of fitness effects (DFE) and the fraction of directly selected sites interact with demographic parameter estimation. The results show that, even after masking functional genomic regions, background selection effects may result in the mis-inference of population growth under models of both constant population size as well as decline. This effect is amplified as the strength of purifying selection and the density of directly selected sites increases, as indicated by the distortion of the site frequency spectrum and levels of nucleotide diversity at linked neutral sites. We also show how simulated changes in background selection effects caused by population size changes can be predicted analytically. We propose a potential method for correcting for the mis-inference of population growth caused by selection. By treating the DFE as a nuisance parameter and averaging across all potential realizations, we demonstrate that even directly selected sites may be used to infer demographic histories with reasonable accuracy.

Keywords: demographic inference, background selection, distribution of fitness effects, MSMC, *fastsimcoal2*, approximate Bayesian computation (ABC)

Running title: Demographic inference with selection

INTRODUCTION

The characterization of past population size change is a central goal of population genomic analysis - with applications ranging from anthropological to agricultural to clinical (see review by Beichman *et al.* 2018). Furthermore, use of an appropriate demographic model provides a necessary null model for assessing the impact of selection across the genome (*e.g.*, Teshima *et al.* 2006; Thornton and Jensen 2007; Jensen *et al.* 2019). Multiple strategies have been proposed for performing demographic inference, utilizing expectations related to levels of variation, the site frequency spectrum, linkage disequilibrium, and within- and between-population relatedness (*e.g.*, Gutenkunst *et al.* 2009; Li and Durbin 2011; Lukic and Hey 2012; Harris and Nielsen 2013; Excoffier *et al.* 2013; Bhaskar *et al.* 2015; Sheehan and Song 2016; Ragsdale and Gutenkunst 2017; Steinrücken *et al.* 2019; Kelleher *et al.* 2019; Speidel *et al.* 2019).

Although many methods perform well when evaluated under the standard assumption of neutrality, it is difficult in practice to assure that the nucleotide sites used in empirical analyses experience neither direct selection nor the effects of selection at linked sites. For example, inference is often performed using intergenic, 4-fold degenerate, or intronic sites. While there is evidence for weak direct selection in all of these categories in multiple organisms (*e.g.*, Haddrill *et al.* 2005; Chamary and Hurst 2005; Andolfatto 2005; Lynch 2007; Zeng and Charlesworth 2010; Choi and Aquadro 2016; Jackson *et al.* 2017), it is also clear that such sites near or in coding regions will also experience background selection (BGS; Charlesworth *et al.* 1993; Charlesworth 2013), and may periodically be affected by selective sweeps as well (Messer and Petrov 2013; Schrider et al. 2016). These effects are known to affect the local underlying effective population size, and alter both the levels and patterns of variation and linkage disequilibrium (Charlesworth et al. 1993; Kaiser and Charlesworth 2009; O'Fallon et al. 2010; Charlesworth 2013; Nicolaisen and Desai 2013; Ewing and Jensen 2016; Johri et al. 2020).

However, commonly-used approaches for performing demographic inference that assume complete neutrality, including *fastsimcoal2* (Excoffier et al. 2013) and MSMC/PSMC (Li and Durbin 2011; Schiffels and Durbin 2014), have yet to be thoroughly evaluated in the light of this assumption, which is likely to be violated in practice. There are, however, some exceptions. Rather than investigating existing software, Ewing and Jensen (2016) implemented an approximate Bayesian (ABC) approach to quantify the impact of BGS effects, demonstrating that weak purifying selection can generate a skew towards rare alleles that would be mis-

interpreted as population growth. Under certain scenarios, this resulted in a many-fold mis-inference of population size change. However, the effects of the density of directly selected sites and the shape of the distribution of fitness effects (DFE), which are probably of great importance, have yet to be considered. Spanning the range of these potential parameter values is important for understanding the implications for empirical application. For example, the proportion of the genome experiencing direct purifying selection can vary greatly between species, with estimates ranging from ~3-8% in humans, to ~12% in rice, to 37-53% in *D. melanogaster*, to 47-68% in *S. cerevisiae* (Siepel et al. 2005; Liang et al. 2018). Further, many organisms have highly compact genomes, with ~88% of the *E. coli* genome (Blattner et al. 1997) and effectively all of many virus genomes, being functional (*e.g.*, >95% of the SARS-CoV-2 genome, Wu *et al.* 2020).

While such estimates allow us to approximate the effects of BGS in some model organisms, in which recombination and mutation rates are well known, it is difficult to predict these effects in the vast majority of study systems. Moreover, while the genome-wide mean of *B*, a widely-used measure of BGS effects that measures the level of variability relative to neutral expectation, can range from ~0.45 in *D. melanogaster* to ~0.94 in humans (Charlesworth 2013; but see Pouyet *et al.* 2018), existing demographic inference approaches are usually applied across organisms without considering this important source of differences in levels of bias. Here, we examine the effects of the DFE shape and functional density on two common demographic inference approaches - the multiple sequentially Markovian coalescent (MSMC) and *fastsimcoal2*. Finally, we propose an extension within the approximate Bayesian computation (ABC) framework to address this issue, treating the DFE as a nuisance parameter and demonstrating greatly improved demographic inference even when using directly selected sites alone.

RESULTS and DISCUSSION

Effects of SNP numbers and genome size on inference under neutral equilibrium

The accuracy and performance of demographic inference was evaluated using two popular methods, MSMC (Schiffels and Durbin 2014) and *fastsimcoal2* (Excoffier et al. 2013). In order

to assess performance, it was first necessary to determine how much genomic information is required to make accurate inference when the assumptions of neutrality are met. Chromosomal segments of varying sizes (10 Mb, 50 Mb, 200 Mb, and 1 Gb) were simulated under neutrality and demographic equilibrium (*i.e.,* constant population size of 5000 diploid individuals) with 100 independent replicates each. For each replicate this amounted to the mean [SD] number of segregating sites for each diploid individual being 1,944 [283], 9,996 [418], 40,046 [957] and 200,245 [1887]; for 50 diploid individuals, these values were 10,354 [225], 51,863 [567], 207,118 [1139] and 1,035,393 [2476] for 10 Mb, 50 Mb, 200 Mb and 1 Gb, respectively. Use of MSMC resulted in incorrect inferences for all segments smaller than 1 Gb (Supp Figure 1). Specifically, very strong recent growth was inferred instead of demographic equilibrium, although ancestral population sizes were correctly estimated. In addition, when 2 or 4 diploid genomes were used for inference, MSMC again inferred a recent many-fold growth for all segment sizes even when the true model was equilibrium, but performed well when using 1 diploid genome for large segments (Supp Figure 1).

When using *fastsimcoal2* to perform demographic inference, parameters were accurately estimated for all chromosomal segment sizes when the correct model (*i.e*., equilibrium) was specified (left panel of Supp Figure 2. However, when model selection was performed using a choice of three models (equilibrium, instantaneous size change, and exponential size change), a minority of replicates of the 10 Mb chromosomal segment incorrectly inferred a size change, although the current population sizes were estimated accurately (middle panel of Supp Figure 2). When the instantaneous bottleneck model was added to the set of competing models, a similarly incorrect model choice was observed at segment sizes less than or equal to 50 Mb (right panel of Supp Figure 2). These results suggest caution when performing inference on smaller regions or genomes, specifically when the number of SNPs are less than ~200,000 per single diploid individual, or less than 1 million per 50 diploid individuals. Extra caution should be used when interpreting population size changes inferred by MSMC when using more than 1 diploid individual.

Given this performance, all further analyses were restricted to characterizing demographic inference on data that roughly matched the structure and size of the human genome - for every diploid individual, 22 chromosomes of size 150 Mb each were simulated, which amounted to roughly 3 Gb of total sequence. Ten independent replicates of each parameter

combination were performed throughout, and inference utilized 1 and 50 diploid individuals for MSMC and *fastsimcoal2,* respectively.

Effect of the strength of purifying selection on demographic inference

In order to test demographic inference in the presence of BGS, all 22 chromosomes were simulated with exons of size 350 bp each, with varying sizes of introns and intergenic regions (see Methods) being used in order to vary the fraction (5%, 10% and 20%) of the genome under selection. Because the strength of selection acting on deleterious mutations affects how far the effects of BGS extend, demographic inference was evaluated for various DFEs (Table 1). The DFE was modelled as a discrete distribution with four fixed classes: $0 \leq |2N_e s| < 1$, $1 \leq |2N_e s| \leq 10$, $10 < |2N_e s| \leq 100$ and $100 < |2N_e s| \leq 2N_e$. The fitness effects of mutations were uniformly distributed within each bin and the DFE shape was altered by varying the proportion of mutations belonging to each fixed class, given by f_0, f_1, f_2, and f_3, respectively (see Methods). Three DFEs highly skewed towards a particular class were initially used to assess the impact of the strength of selection on demographic inference (with the remaining mutations equally distributed amongst the other three classes):

DFE1: a DFE in which 70% of mutations have weakly deleterious fitness effects (*i.e.*, $f_1 = 0.7$),

DFE2: a DFE in which 70% of mutations have moderately deleterious fitness effects (*i.e.*, $f_2 = 0.7$), and

DFE3: a DFE in which 70% of mutations have strongly deleterious fitness effects (*i.e.*, $f_3 = 0.7$).

In order to understand the effects of BGS, exonic sites were masked, and only linked neutral intergenic sites were used for demographic inference. The three demographic models examined were (1) demographic equilibrium, (2) a 30-fold exponential growth, mimicking the recent growth experienced by European human populations, and (3) ~6-fold instantaneous decline, mimicking the out-of-Africa bottleneck in human populations (Figure 1a). Although these models were parameterized using previous estimates of human demographic history (Supp Table 1; Gutenkunst *et al.* 2009), these basic demographic scenarios are applicable to many organisms, although the magnitudes of population size changes in this case may represent an extreme.

Under demographic equilibrium, when 20% of the genome experiences direct selection (with masking of the directly selected sites), we found the true population size to be

underestimated, as well recent population growth mis-inferred (Figure 1), with a larger bias in MSMC than *fastsimcoal2*. Stronger growth is inferred with larger fitness effects of mutations. Conversely, when the true demographic model is characterized by recent 30-fold growth, demographic inference is accurate and performs equally well for both MSMC and *fastsimcoal2*, with the exception of a slight underestimation of the ancestral population size for all DFE types. When the true model is population decline, weakly deleterious mutations alone did not affect inference drastically and it was possible to recover the true model. However, moderately and strongly deleterious mutations resulted in an underestimation of population size and an inference of strong growth, to the extent that population decline would be misinterpreted as growth. We further tested the effect of BGS on demographic inference when changes in population size were less severe, namely, when population growth and decline was only 2-fold, with qualitatively similar results (Supp Figure 3).

Finally, given the strong evidence that most organisms have a bi-modal DFE with a significant proportion of strongly deleterious or lethal mutations (Sanjuán 2010; Jacquier et al. 2013; Kousathanas and Keightley 2013; Bank et al. 2014; Charlesworth 2015), we investigated the effect of this strongly deleterious class further. Thus, for comparison with the above, we simulated a rather extreme case in which 30% or 50% of exonic mutations are strongly deleterious with fitness effects uniformly sampled between $100 \leq 2N_{\text{anc}}s \leq 2N_{\text{anc}}$, with the remaining mutations being neutral (*i.e.*, DFE5 and DFE6; see Table 1). As with the above results, both equilibrium and decline models were falsely inferred as growth, with an order of magnitude underestimation of the true population size (Figure 2).

In sum, neglecting BGS frequently results in the inference of population growth, almost regardless of the true underlying demographic model.

Effects of density and inclusion/exclusion of directly selected sites on inference

Although we have shown that the presence of purifying selection biases demographic inference, the extent of mis-inference necessarily depends on the fraction of the genome experiencing direct selection. We therefore compared models in which 5%, 10% or 20% of the genome was functional. For this comparison, equal proportions of mutations in each DFE bin were assumed (*i.e.,* $f_0 = f_1 = f_2 = f_3 = 0.25$) corresponding to DFE4 (Table 1). As before, when the true model was exponential growth, inference was unbiased, with a slight underestimation of ancestral

population size when 20% of the genome experiences selection (Figure 3). Population decline was inferred reasonably well if less than 10% of the genome experiences direct selection, but could be mis-inferred as growth with greater functional density, as shown in Figure 3. Similarly, the extent to which population size is under-estimated at demographic equilibrium increases with the fraction of the genome under selection. Finally, it is noteworthy that many changes in population size that were falsely inferred were greater than 2-fold in size, suggesting the need for great caution when inferring such changes from real data.

Importantly, the results presented do not significantly differ between inference performed while including directly selected sites (*i.e.*, no masking of functional regions; Supp Figure 4) versus inference performed using linked neutral sites (*i.e.*, masking functional regions; Figures 1-3). These results suggest that the exclusion of exonic sites, which is often assumed to provide a sufficiently neutral dataset to enable accurate demographic inference, is not necessarily a satisfactory solution unless gene density is low.

Effect of heterogeneity in recombination rates, mutation rates, and repeat masking

Variation in recombination and mutation rates, as well as the masking of repeat regions, may also affect demographic inference procedures. We evaluated this issue by simulating heterogeneity in both mutation and recombination rates (based on estimated human genome maps, as described in the Methods section), and masking 10% of each simulated segment drawing from the empirical distribution of repeat lengths in the human genome (Supp Figure 5). In general, inferences under neutrality (Supp Figures 6-8) as well as under BGS (Supp Figures 9-11) were unaffected under all demographic models. These investigations suggest that such demographic inference is robust to genome-wide variation in rates of recombination and mutation, as well as the presence of repeat elements. Thus, serious mis-inference is more likely to be caused by selection. These observations also suggest that simulations performed with mean rates of recombination and mutation, as performed in this study, are sufficient to evaluate biases caused by BGS.

Effects of BGS on diversity and the SFS under various demographic models: theoretical expectations versus simulation results

To better understand how BGS can lead to different biases in the inference of population history, we investigated the extent of BGS effects under all three demographic models, with respect to both the reduced diversity relative to neutrality, as well as the shape of the SFS at linked neutral sites. First, we found that B, the diversity relative to the neutral expectation, differed among demographic scenarios, disproportionately amplifying mis-inference under equilibrium and decline (Figure 4). After a population decline, B was lower than that before the size change; while after population expansion, B increased relative to that in the ancestral population, sometimes approaching 1 (Figure 4). This may seem paradoxical, given that the magnitude of the scaled selection coefficient ($2N_es$) decreases with decreasing N_e (*i.e.*, the efficacy of purifying selection decreases, and could thus be expected to result in larger values of B under population decline). Conversely, with increasing N_e, B may be reduced.

However, these expectations apply only once a population has maintained a given N_e for sufficient time such that equilibrium has been approached. During the initial stages of population size change, and shortly afterwards, the dynamics of B tend to show a trend opposite to this long-term expectation (see also Figure 5 of Torres *et al.* 2020). This is because differences in N_e caused by different initial levels of BGS cause differences in the rates of response to changes in population size – a small value of N_e (corresponding to low B) results in a faster response compared with a high value (Fay and Wu 1999; Hey and Harris 1999; Pool and Nielsen 2007; Pool and Nielsen 2009; Campos et al. 2014; Torres et al. 2020). The relative diversity values observed with different initial equilibrium B values after a short period of population size change may thus be very different from both the initial and final equilibrium values, so that the apparent B values estimated by comparing diversities with and without BGS differ from the equilibrium values. The overall effect is that there is an apparent increase in B immediately following a population decline, and a decrease immediately following an expansion. Analytical models describing these effects are presented in the Appendix. These models used the simulated values of B at equilibrium before the population size changes to predict the apparent B values at the ends of the periods of size change (see the Methods and Appendix). It can be seen from Figure 4 that there is good agreement between these predictions and the simulation results.

Because several demographic estimation methods are based on fitting a demographic model to the SFS, it is also of interest to understand whether BGS can skew the SFS to different extents under different demographic models. Although it is well known that BGS causes a skew of the SFS towards rare variants under equilibrium models (Charlesworth et al. 1995; Nicolaisen and Desai 2013), the effect of BGS on the SFS with population size change has not been much explored (but see Johri *et al.* 2020 and Torres *et al.* 2020). As shown in Figure 5, with a population size decline, the SFS of derived alleles is more skewed towards rare variants when BGS is operating, especially when B is initially small, since the effects of BGS work in opposition to the effects of the population size reduction. This difference in the left skew of the SFS with and without BGS is much less noticeable in the case of population expansion, since here the effects of BGS and the expansion act in a similar direction.

As with the estimates of the apparent B values discussed above, analytical predictions of expected SFS after an instantaneous/ exponential change in population size can be made, using the values of B at equilibrium before the population size change (see the Methods), using the formulae of Polanski and Kimmel (2003) and Polanski *et al.* (2003) for the purely neutral case, as described in the Methods section. Although the shape of the SFS is affected by both demography and BGS, the impact of BGS is often comparatively small. Figure 5 shows that the overall shape of the SFS is predicted reasonably well by the analytical results, although deviations are to be expected for the rare allele classes, which are the most sensitive to demographic change and selection. Overall, the results imply that BGS is more likely to bias demographic inference post-decline compared with post-increase, consistent with the performance of the methods described above. However, it should be noted that the exact patterns observed will depend on the timing of population size changes relative to the time of sampling, as well as the value of B before the size change. For example, with a past step increase in population size, a genomic region with a sufficiently low B may not show signs of an expansion, because all coalescent events will have been completed before the time of expansion. The patterns described here thus represent only a small subset of the possibilities. In addition, all else being equal, in populations with large long-term population sizes (and thus low values of B), BGS would be expected to result in even larger biases than those observed here.

A potential solution: averaging across all possible DFEs

As shown above, demographic inference can be strongly affected by currently unaccounted for BGS effects, as well as by direct purifying selection. A potential solution is thus to correct for these effects when performing inference of population history. A widely-used approach to estimating direct selection effects, DFE-alpha, takes a stepwise approach to inferring demography, by using a presumed neutral class (synonymous sites); conditional on that demography, it then estimates the parameters of the DFE (Keightley and Eyre-Walker 2007; Eyre-Walker and Keightley 2009; Schneider et al. 2011; Keightley and Jackson 2018). However, this approach does not include the possibility of effects of selection at linked sites, which can result an over-estimate of population growth, as well as general mis-inference of the DFE (Johri et al. 2020).

Building on this idea, Johri et al. (2020) recently proposed an approach that includes both direct and background effects of purifying selection, simultaneously inferring the deleterious DFE and demography. By utilizing the decay of BGS effects around functional regions, they demonstrated high accuracy under the simple demographic models examined. Moreover, the method makes no assumptions about the neutrality of synonymous sites, and can thus be used to estimate selection acting on these sites, as well as in non-coding functional elements. However, this computationally-intensive approach is specifically concerned with jointly inferring the DFE and demographic parameters. As such, if an unbiased characterization of the population history is the sole aim, this procedure may be needlessly involved. We thus here examine the possibility of rather treating the DFE as an unknown nuisance parameter, averaging across all possible DFE shapes, in order to assess whether demographic inference may be improved simply by correcting for these selection effects without inferring their underlying parameter values. This approach utilizes functional (*i.e.*, directly selected) regions, a potential advantage in populations for which only coding data may be available (*e.g.*, exome-capture data; see Jones and Good 2016), or more generally in organisms with high gene densities.

In order to illustrate this approach, a functional genomic element was simulated under demographic equilibrium, 2-fold exponential population growth and 2-fold exponential population decline with four different DFE shapes (as described previously, and shown in Figure 6). A number of summary statistics were calculated (see Methods) for the entire functional region. Inference was first performed assuming strict neutrality, and inferring a one-epoch size

change (thus estimating the ancestral (N_{anc}) and current population sizes (N_{cur})). As was found with the other inference approaches examined, population sizes were underestimated and a false inference of population growth was observed in almost all cases when selective effects are ignored (Figure 6).

Next, the assumption of neutrality was relaxed, and mutations were simulated with fitness effects characterized by a discrete DFE, with the same fitness classes given above (f_0, f_1, f_2, f_3). Values for f_i were drawn from a uniform prior between 0 and 1, such that $\sum f_i = 1$. Note that no assumptions were made about which sites in the genomic region were functionally important, or regarding the presence/absence of a neutral class. These directly selected sites were then used to infer demographic parameters. We found that, by varying the shape of the DFE, averaging across all realizations, and estimating only parameters related to population history, highly accurate inference of modern and ancestral population sizes is possible (Figure 6). These results demonstrate that, even if the true DFE of a population is unknown (as will always be the case in reality), it is possible to infer demographic history with reasonable accuracy by approximately correcting for these selective effects.

CONCLUSION

While commonly used approaches for inferring demography assume neutrality and independence among segregating sites, it is very difficult to verify those assumptions empirically. In addition, there is considerable evidence for wide-spread effects of selection on linked sites in many commonly studied organisms (Hernandez et al. 2011; Cutter and Payseur 2013; Williamson et al. 2014; Elyashiv et al. 2016; Campos et al. 2017; Booker and Keightley 2018; Pouyet et al. 2018; Torres et al. 2018; Castellano et al. 2020). As such, we explored how violations of the assumption of neutrality may affect demographic inference, particularly with regard to the underlying strength of purifying selection and the genomic density of directly selected sites. Generally speaking, the neglect of these effects (*i.e.*, background selection) results in an inference of population growth, with the severity of the growth model roughly scaling with selection strength and density. Thus, when the true underlying model is in fact growth, demographic mis-inference is not particularly severe; when the true underlying model is constant

size or decline, the mis-inference can be extreme, with a many-fold underestimation of population size.

It is important to note that BGS effects extend to genomic distances in a way that is positively related to the strength of purifying selection. For instance, strongly and moderately deleterious mutations affect patterns of diversity at large genomic distances, whereas mildly deleterious mutations primarily skew allele frequencies at adjacent sites. Thus, if intergenic regions further away from exons are used to perform demographic inference, it is predominantly strongly deleterious mutations that are likely to bias inferences. In contrast, if synonymous sites are used to infer demographic history, mildly deleterious mutations will be most important. Thus, as we here focused on relatively sparsely-coding genomes (resembling human-like gene densities) and used intergenic sites for inference, moderately and strongly deleterious mutations resulted in more severe mis-inference. In addition, the effect of decay of BGS due to mildly deleterious mutations depends on multiple parameters. For instance, with an exon of length 500 bp and *Drosophila*-like parameters ($N_e = 10^6$; recombination rate = mutation rate = 10^{-8} / site / generation), B will increase from 0.53 (at 10 bases from the end of the exon) to 0.94 at a distance of 1000 bases. On the other hand, with human-like parameters ($N_e = 10^4$; recombination rate = mutation rate = 10^{-8} / site / generation),) the corresponding change in B is only 0.981 to 0.982 (Supp Table 2). Thus, mildly deleterious mutations will have drastically different effects in this regard depending on the underlying population parameters. Hence, a large impact of selection is expected when such approaches are applied to synonymous sites in smaller and more compact genomes with higher gene densities and a larger input of deleterious mutations at closely linked sites.

Comparing the two inferences methods investigated here, it appears that *fastsimcoal2* is less prone to inferring false fluctuations in population size caused by BGS. However, both methods falsely infer growth when it is absent, with increasing severity as the density of coding regions increases. The times of population growth inferred by both methods appear to be affected in unpredictable ways. Further, we observed little difference in performance when using all SNPs relative to when SNPs are thinned to be separated by 5kb (Supp Figure 12), presumably because the models investigated do not generate strong LD. Overall, the degree of mis-inference caused by a neglect of BGS is largely similar between the two methods.

However, it is noteworthy that even when all sites are strictly neutral, or only 5% of the genome experiences direct selection, demographic equilibrium is mis-estimated by MSMC as a series of size changes. The pattern of these erroneous size changes lend a characteristic shape to the MSMC curve (*i.e.*, ancient decline and recent growth) which appears to resemble the demographic history previously inferred for the Yoruban population (Schiffels and Durbin 2014), including the time at which changes in population size occurred (Supp Figure 13). Previous work has demonstrated that the resulting demographic model does not in fact fit the observed SFS in the Yoruban population (Beichman et al. 2017; Lapierre et al. 2017). A similar shape has also been inferred in the vervet subspecies (Warren *et al.* 2015; Figure 4), in passenger pigeons (Hung *et al.* 2014; Figure 2), in elephants (Palkopoulou *et al.* 2018; Figure 4), in *Arabidopsis* (Fulgione *et al.* 2018; Figure 3), and in grapevines (Zhou *et al.* 2017; Figure 2A).

Although the inferred population size fluctuations under simulated neutrality are only ~1.2-fold, in most empirical applications the fluctuations are of a somewhat larger magnitude (~ 2-fold in pigeons, *Arabidopsis*, and grapevines). Nonetheless, this neutral performance of MSMC under demographic equilibrium is concerning, and adds to the other previously published cautions concerning the interpretation of MSMC results. For example, Mazet *et al*. (2016) and Chikhi *et al*. (2018) demonstrated that under constant population size with hidden structure, inference may suggest false size change (see also Orozco-terWengel 2016). In addition, MSMC has been reported to falsely infer growth prior to instantaneous bottlenecks (Bunnefeld et al. 2015). In addition, we observed that if insufficient genomic data is utilized, or more than one diploid genome is used to perform inference, MSMC falsely infers recent growth of varying magnitudes (as previously observed by Beichman et al. 2017).

In sum, we find that the effects of purifying and background selection result in similar demographic mis-inference across approaches, and that masking functional sites does not yield accurate parameter estimates. In order to side-step many of these difficulties, our proposed approach of inferring demography by averaging selection effects across all possible DFE shapes within an ABC framework appears to be promising. Utilizing only functional regions, we found a great improvement in accuracy, without making any assumptions regarding the true underlying shape of the DFE or the neutrality of particular classes of sites. As such, this approach represents a more computationally efficient avenue if only demographic parameters are of interest, and

ought to be particularly useful in the great majority of organisms in which unlinked neutral sites either do not exist, or are difficult to identify and verify.

METHODS

Simulations: Simulations were performed using SLiM 3.1 (Haller and Messer 2019) with 10 replicates per evolutionary scenario. For every replicate, 22 chromosomes of 150Mb each were simulated, totaling ~3 Gb of information per individual genome (similar to the amount of information in a human genome). Within each chromosome, 3 different types of regions were simulated, representing non-coding intergenic, intronic, and exonic regions. Based on the NCBI RefSeq human genome annotation, downloaded from the UCSC genome browser for hg19 (http://genome.ucsc.edu/; Kent *et al.* 2002), mean values of exon sizes and intron numbers per gene were calculated. To represent mean values for the human genome (Lander et al. 2001), each gene was comprised of 8 exons and 7 introns, and exon lengths were fixed at 350 bp. By varying the lengths of the intergenic and intronic regions, three different genomic configurations with varying densities of functional elements were simulated and compared - with 5%, 10% and 20% of the genome being under direct selection - hereafter referred to as genome5, genome10, and genome20, respectively. Genome5 was comprised of introns of 3000 bp and intergenic sequence of 31000 bp, genome10 of introns of 1500 bp and intergenic sequence of 15750 bp, while genome20 was comprised of introns of 600 bp and intergenic sequence of 6300 bp. The total chromosome sizes of these genomes were approximately 150 Mb (150,018,599 bp, 150,029,949 bp, 150,003,699 bp in genome5, 10, and 20, respectively) with 2737, 5164, and 11278 genes per chromosome in genome5, 10 and 20, respectively. In order to be conservative with respect to the performance of existing demographic estimators, intronic and intergenic regions were assumed to be neutral.

Recombination and mutation rates were assumed to be equal at 1×10^{-8} /site / generation. Neither crossover interference (see the discussion in Campos and Charlesworth 2019) nor gene conversion were modeled. Exonic regions in the genomes experienced direct purifying selection given by a discrete DFE comprised of 4 fixed classes (Johri et al. 2020), whose frequencies are denoted by f_i: f_0, with $0 \leq 2N_e s < 1$ (*i.e.*, effectively neutral mutations), f_1, with $1 \leq 2N_e s < 10$ (*i.e.*, weakly deleterious mutations), f_2, with $10 \leq 2N_e s < 100$ (*i.e.*, moderately deleterious

mutations), and f_3, with $100 \leq 2N_e s < 2N_e$ (*i.e.*, strongly deleterious mutations), where N_e is the effective population size and s is the reduction in fitness of the mutant homozygote relative to wild-type. Within each bin, the distribution of s was assumed to be uniform. All mutations were assumed to be semi-dominant. In all cases, the N_e corresponding to the DFE refers to the ancestral effective population size. Six different types of DFE were simulated: DFE1: a DFE skewed largely towards mildly deleterious mutations, given by f_0=0.1, f_1=0.7, f_2=0.1, f_3=0.1; DFE2: a DFE skewed towards moderately deleterious mutations, f_0=0.1, f_1=0.1, f_2=0.7, f_3=0.1; DFE3: a DFE skewed towards strongly deleterious mutations, f_0=0.1, f_1=0.1, f_2=0.1, f_3=0.7; DFE4: a DFE with equal proportions of all mutations, f_0=0.25, f_1=0.25, f_2=0.25, f_3=0.25; DFE5: a DFE with equal proportions of neutral and strongly deleterious mutations, f_0=0.5, f_1=0.0, f_2=0.0, f_3=0.5' and DFE6: a DFE with a majority of neutral mutations and a minority of strongly deleterious mutations, f_0=0.7, f_1=0.0, f_2=0.0, f_3=0.3.

Three different demographic models were tested for each of these DFEs (Supp Table 1): 1) demographic equilibrium, 2) recent exponential 30-fold growth, resembling that estimated for the human CEU population (Gutenkunst et al. 2009), and 3) ~6-fold instantaneous decline, resembling the out-of-Africa bottleneck in humans (Gutenkunst et al. 2009).

Running MSMC: In order to quantify the effect of purifying selection on demographic inference, we used entire chromosomes generated by SLiM to generate input files for MSMC. For comparison, and to quantify the effect of BGS alone on demographic inference, we masked the exonic regions to generate input files. For all parameters, MSMC was performed on a single diploid genome, as the results for this case were the most accurate (Supp Figure 1). Input files were made using the script ms2multihetsep.py provided in the msmc-tools-Repository downloaded from https://github.com/stschiff/msmc-tools. MSMC1 and 2 were run as follows: *msmc_1.1.0_linux64bit -t 5 -r 1.0 -o output_genomeID input_chr1.tab input_chr2.tab ... input_chr22.tab.* Population sizes obtained from MSMC were plotted up to the maximum number of generations obtained from MSMC, and the final value of the ancestral population size was extended indefinitely as a dashed line.

Running Fastsimcoal2: In order to minimize the effects of linkage disequilibrium (LD), only SNPs separated by 5 kb were used for inference, following Excoffier et al. (2013). Inference was

also performed by including all SNPs in order to assess the impact of violating the assumption of no LD on inference. Site frequency spectra (SFS) were obtained for both sets of SNPs for all 10 replicates of every combination of demographic history and DFE. SNPs from all 22 chromosomes were pooled together to calculate the SFS. *Fastsimcoal2* was used to fit each SFS to 4 distinct models: (a) equilibrium, which estimates only a single population size parameter (N); (b) instantaneous size change (decline/growth), which fits 3 parameters - ancestral population size (N_{anc}), current population size (N_{cur}), and time of change (T); (c) exponential size change (decline/growth), which also estimates 3 parameters - N_{anc}, N_{cur} and T; and (d) an instantaneous bottleneck model with 3 parameters – N_{anc}, intensity, and time of bottleneck. The parameter search ranges for both ancestral and current population sizes in all cases were specified to be uniformly distributed between 100-500000 individuals, while the parameter range for time of change was specified to be uniform between 100-10000 generations in all models. The intensity of the bottleneck, as specified by the population size during the reduction, was also sampled uniformly from the range 100-500000 individuals. The following command line was used to run *fastsimcoal2*:

fsc26 -t demographic_model.tpl -n 150000 -d -e demographic_model.est -M -L 50 -q,

Model selection was performed as recommended by Excoffier et al. (2013). For each demographic model, the maximum of maximum likelihoods from all replicates was used to calculate the Akaike Information Criterion (AIC) = 2 × number of parameters – 2 × ln(likelihood). The relative likelihoods (Akaike's weight of evidence) in favor of the i^{th} model was then calculated by:

$$w(i) = \frac{e^{-0.5\Delta_i}}{\sum_{j=1}^{4} e^{-0.5\Delta_j}}$$

where $\Delta_i = AIC_i - AIC_{min}$. The model with the highest relative likelihood was selected as the best model, and the parameters estimated using that model were used to plot the final inferred demography.

Simulations of variable recombination and mutation rates, and repeat masking: In order to simulate variation in recombination and mutation rates, all 22 chromosomes were simulated by mimicking chromosome 6 (~171Mb) of the human genome. Recombination rates obtained from Yoruban populations were obtained from the UCSC genome browser, while the mutation rate

map (https://molgenis26.target.rug.nl/downloads/gonl_public/mutation_rate_map/release2/) was assumed to correspond to estimates obtained from *de novo* mutations (Francioli et al. 2015), as in Castellano *et al.* (2020). Absolute values of mutation rates were normalized in order to maintain the mean mutation rate across the genome at $\sim 1.0 \times 10^{-8}$ per site per generation. Recombination and mutation rate estimates were taken from positions of approximately 10 Mb to 160 Mb, with the recombination map starting at 10010063 bp and the mutation map starting at 10010001 bp. Regions with missing data for either of the two estimates were simulated with rates corresponding to the previous window, except for the case of centromeres in which no recombination was assumed. In order to understand the effect of excluding centromeric regions in empirical studies, the 4Mb region corresponding to the centromere was masked, corresponding to 48.5 to 52.5 Mb of the simulated 150Mb chromosomes. In order to evaluate the effect of masking repeat regions, random segments comprising 10% of each chromosome were masked. The lengths of these segments were drawn from the lengths of repeat regions found in the human genome (Supp Figure 5), as obtained from the repeat regions in the *hg19* assembly of the human genome from the UCSC genome browser.

Performing inference by approximate Bayesian computation (ABC): ABC was performed using the R package "abc" (Csilléry et al. 2010), and non-linear regression aided by a neural net (used with default parameters as provided by the package) was used to correct for the relationship between parameters and statistics (Johri et al. 2020). To infer posterior estimates, a tolerance of 0.1 was applied (*i.e.*, 10% of the total number of simulations were accepted by ABC in order to estimate the posterior probability of each parameter). The weighted medians of the posterior estimates for each parameter were used as point estimates. ABC inference was performed under two conditions: (1) complete neutrality, or (2) the presence of direct purifying selection. In both cases only 2 parameters were inferred - ancestral (N_{anc}) and current (N_{cur}) population sizes. However, in scenario 2, the shape of the DFE was also varied. Specifically, the parameters f_0, f_1, f_2, and f_3 were treated as nuisance parameters and were sampled such that $0 \leq f_i \leq 1$, and $\Sigma_i f_i = 1$, for $i = 0$ to 3. In addition, in order to limit the computational complexity involved in the ABC framework, values of f_i were restricted to multiples of 0.05 (*i.e.*, $f_i \in \{0.0, 0.05, 0.10, \ldots, 0.95, 1.0\}\ \forall\ i$), which allowed us to sample 1,771 different DFE realizations. Simulations were performed with functional genomic regions, and the demographic model was

characterized by 1-epoch changes in which the population either grows or declines exponentially from ancestral to current size, beginning at a fixed time in the past.

For the purpose of illustration, and for a contrast with the human-like parameter set above, parameters for ABC testing were selected to resemble those of *D. melanogaster* African populations. Priors on ancestral and current population sizes were drawn from a uniform distribution between 10^5-10^7 diploid individuals, while the time of change was fixed at 10^6 ($\sim N_e$) generations. In order to simulate functional regions, 94 single-exon genes, as described in Johri *et al*. (2020) and provided in https://github.com/paruljohri/BGS_Demography_DFE/blob/master/DPGP3_data.zip, were simulated with recombination rates specific to those exons (https://petrov.stanford.edu/cgi-bin/recombination-rates_updateR5.pl) (Fiston-Lavier et al. 2010; Comeron et al. 2012). Mutation rates were assumed to be fixed at 3×10^{-9} per site per generation (Keightley et al. 2009; Keightley et al. 2014).

All parameters were scaled by the factor 320 in order to decrease computational time, using the principle first described by Hill and Robertson (1966), and subsequently by others (Comeron and Kreitman 2002; Hoggart et al. 2007; Kaiser and Charlesworth 2009; Kim and Wiehe 2009; Uricchio and Hernandez 2014; Campos and Charlesworth 2019). The scaled population sizes thus ranged between ~300–30000 and were reported as scaled values in the main text. One thousand replicate simulations were performed for every parameter combination (N_{anc}, N_{cur}, f_0, f_1, f_2, f_3); for performing ABC inference, 50 diploid genomes were randomly sampled without replacement, and summary statistics were calculated using pylibseq 0.2.3 (Thornton 2003). Means and variances (between replicates) of the following summary statistics were calculated across the entire exonic region: nucleotide site diversity (π), Watterson's θ, Tajima's D, Fay and Wu's H (both absolute and normalized), number of singletons, haplotype diversity, LD-based statistics (r^2, D, D'), and divergence (*i.e*., number of fixed mutations per site per generation after the burn-in period). As opposed to the above examples, in this inference scheme only exonic data (*i.e*., directly selected sites) were utilized. Test datasets were generated in exactly the same fashion as described above.

Analytical expectations for the relative site frequencies: To compute the expected relative frequencies of site frequency classes, the approach of Polanski and Kimmel (2003) was

584 followed. They describe a method for computing the "probability that a SNP has *b* mutant
585 bases", which is equivalent to the site frequency spectrum (SFS) of derived variants. This
586 method (their equations 3-10) allows for the specification of arbitrary population size histories
587 and sample sizes. For reasons of computational precision, a sample size of 10 diploid genomes
588 was chosen. The demographic scenarios detailed in Supplementary Table 1 were implemented as
589 piecewise functions of the effective population size (counting haploid genomes), and the effect
590 of BGS was included by scaling these functions by values of *B* before population size change as
591 obtained from the forwards-in-time simulations described above. A Mathematica notebook
592 detailing these results, will be made available upon publication (see data availability statement).
593 In addition, analytical expressions can be obtained for pairwise diversity values when there are
594 step changes or exponential growth in population size, as described in the Appendix and in an
595 example program that calculates diversity values after exponential growth.
596
597 ***Data availability***: The following data will be made publicly available upon acceptance of the
598 manuscript: (1) Scripts used to perform simulations; (2) Input files used to run *fastsimcoal2*; (3)
599 Scripts used for plotting; (4) Plotted results of MSMC and *fastsimcoal2* for all models and
600 scenarios tested in this work; (5) A Mathematica (version 12.1) notebook detailing calculations
601 of analytical expectations for the relative SFS; (6) An example program (Fortran script)
602 demonstrating how to obtain analytical expressions for values of *B* after exponential growth. All
603 supplemental files will be made publicly available at
604 https://github.com/paruljohri/demographic_inference_with_selection.
605
606
607 **Acknowledgements**

608 We would like to thank Susanne Pfeifer for helpful discussions related to this project, and for
609 feedback on the manuscript. This research was conducted using resources provided by Research
610 Computing at Arizona State University (http://www.researchcomputing.asu.edu) and the Open
611 Science Grid, which is supported by the National Science Foundation and the U.S. Department
612 of Energy's Office of Science. This work was funded by National Institutes of Health grant
613 R01GM135899 to JDJ.

APPENDIX

There are two simple scenarios for population size change for which simple explicit expressions for the expected pairwise coalescent time or diversity can be obtained, without using the methodology of Polanski and Kimmel (2003) and Polanski *et al.* (2003) – a step change in N or an exponential growth in N. First consider the coalescent process for a step change, where the current and initial effective population sizes are denoted by N_{e1} and N_{e0}, respectively. Let B be the background selection parameter at the start of the process of change, corresponding to effective size N_{e0}. For convenience, time is scaled in units of $2N_{e1}$ generations, and the time of the change in population size on this scale is denoted by T_0, counting back from the present time, $T = 0$. T_0 is assumed to be sufficiently small that B remains approximately constant during the period since the change in size. Denote the ratio N_{e0}/N_{e1} by R. The derivation for the case of a step change in population size is similar to that given by Pool and Nielsen (2009) for the purpose of comparing X chromosomes and autosomes.

Between times T and T_0, coalescence occurs at a rate B^{-1} on the chosen timescale, so that the contribution from this period to the net coalescent time for a pair of alleles sampled at $T = 0$ is:

$$B^{-1}\int_0^{T_0} T\exp(-B^{-1}T)\,\mathrm{d}T = B - B\exp(-B^{-1}T_0) - T_0\exp(-B^{-1}T_0)$$

There is a probability of $\exp(-B^{-1}T_0)$ that there is no coalescence when T lies between 0 and T_0, after which coalescence occurs at a rate $1/BR$, giving a net contribution to the coalescence time of:

$$(BR + T_0)\exp\,(-B^{-1}T_0)$$

The net coalescence time for the stepwise change with BGS is given by the sum of these two expressions:

$$B[1 + (R - 1)\exp(-B^{-1}T_0)] \qquad (1a)$$

If this expression is compared to the corresponding equation with $B = 1$, the apparent value of B at the time of sampling of the pair of alleles is given by:

$$B_s = \frac{B[1+(R-1)\exp(-B^{-1}T_0)]}{[1+(R-1)\exp(-T_0)]} \quad (1b)$$

Next, consider a process of exponential change in population size, starting at an initial effective size of N_{e0} at t_0 generations in the past and ending at size N_{e1}, such that the instantaneous growth rate r per generation is r=equal to $\ln(N_{e1}/N_{e0})/t_0$. The effective population size at time t in the past is $N_e(t) = N_{e1}\exp(-rt)$; with BGS, the rate of coalescence at time t is $1/BN_e(t)$. As before, the BGS parameter is assumed to remain constant over the period of population size change. It follows that the probability of no coalescence by generation t in the past is:

$$P_{nc}(t) = \exp\left[-\int_0^t (2BN_{e1})^{-1}\exp(rt)\,\mathrm{d}t\right] = \exp[c^{-1}(1-e^{rt})] \quad (2)$$

where $c = 2BNe_1r$.

The pre-growth period with $t > t_0$ contributes an expected coalescent time of $(2BN_{e0} + t_0)P_{nc}(t_0)$, on the scale of generations.

Following Slatkin and Hudson (1991), to obtain the contribution from the period with $t > t_0$, it is convenient to measure time as $\tau = rt$. The probability of coalescence between τ and $\tau + \mathrm{d}\tau$ is then given by:

$$P_c(\tau) = c^{-1}e^{\tau}\exp[c^{-1}(1-e^{\tau})]\,\mathrm{d}\tau \quad (3)$$

The contribution from this period to the expected coalescent time is given by the integral of $\tau\,P_c(\tau)$ between 0 and τ_0. Following Slatkin and Hudson (1991), by transforming to $u = \exp(\tau)$, this contribution can be expressed as the following integral:

$$\bar{\tau}_1 = c^{-1}e^{c^{-1}}\int_1^{u_0}\ln(u)e^{-uc^{-1}}du \quad (4)$$

This integral can easily be evaluated numerically. The corresponding mean coalescent time on the scale of generations is obtained by division by r, and the result can be added to $(2BN_{e0} + t_0)P_{nc}(t_0)$, yielding the net expected coalescent time. By dividing the resulting

673 expression by the corresponding expression with $B = 1$, the apparent BGS effect at the time of
674 sampling can be obtained, in the same way as for the step change model.
675
676
677 **FIGURES AND TABLES**
678
679
680 **Table 1**: Proportion (f_i) of mutations in each class of the discrete distribution of fitness effects
681 (DFE) simulated in this study.

	f_0	f_1	f_2	f_3
DFE1	0.1	0.7	0.1	0.1
DFE2	0.1	0.1	0.7	0.1
DFE3	0.1	0.1	0.1	0.7
DFE4	0.25	0.25	0.25	0.25
DFE5	0.5	0.0	0.0	0.5
DFE6	0.7	0.0	0.0	0.3

682

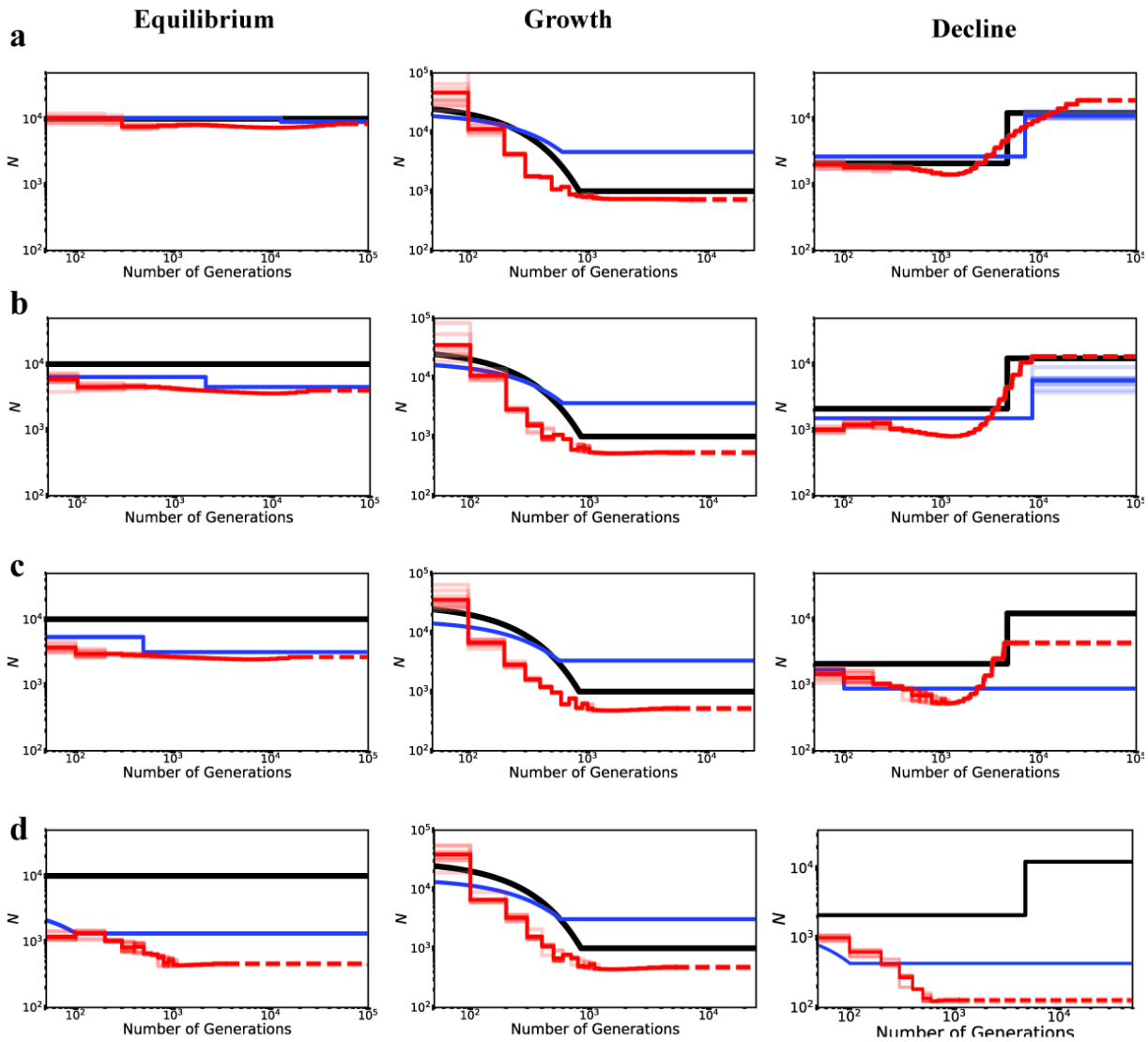

Figure 1: Inference of demography by MSMC (red lines; 10 replicates) and *fastsimcoal2* (blue lines; 10 replicates) with and without BGS, under demographic equilibrium (left column), 30-fold exponential growth (middle column), and ~6-fold instantaneous decline (right column). The true demographic models are depicted as black lines, with the x-axis origin representing the present day. (a) All genomic sites are strictly neutral. (b) Exonic sites experience purifying selection specified by a DFE comprised largely of weakly deleterious mutations (DFE1: $f_0 = 0.1$, $f_1 = 0.7$, $f_2 = 0.1$, $f_3 = 0.1$). (c) Exonic sites experience purifying selection specified by a DFE comprised largely of moderately deleterious mutations (DFE2: $f_0 = 0.1$, $f_1 = 0.1$, $f_2 = 0.7$, $f_3 = 0.1$). (d) Exonic sites experience purifying selection specified by a DFE comprised largely of strongly deleterious mutations (DFE3: $f_0 = 0.1$, $f_1 = 0.1$, $f_2 = 0.1$, $f_3 = 0.7$). Exons represent 20% of the genome, and exonic sites were masked/excluded when performing demographic inference, quantifying the effects of BGS alone. The dashed lines represent indefinite extensions of the ancestral population sizes.

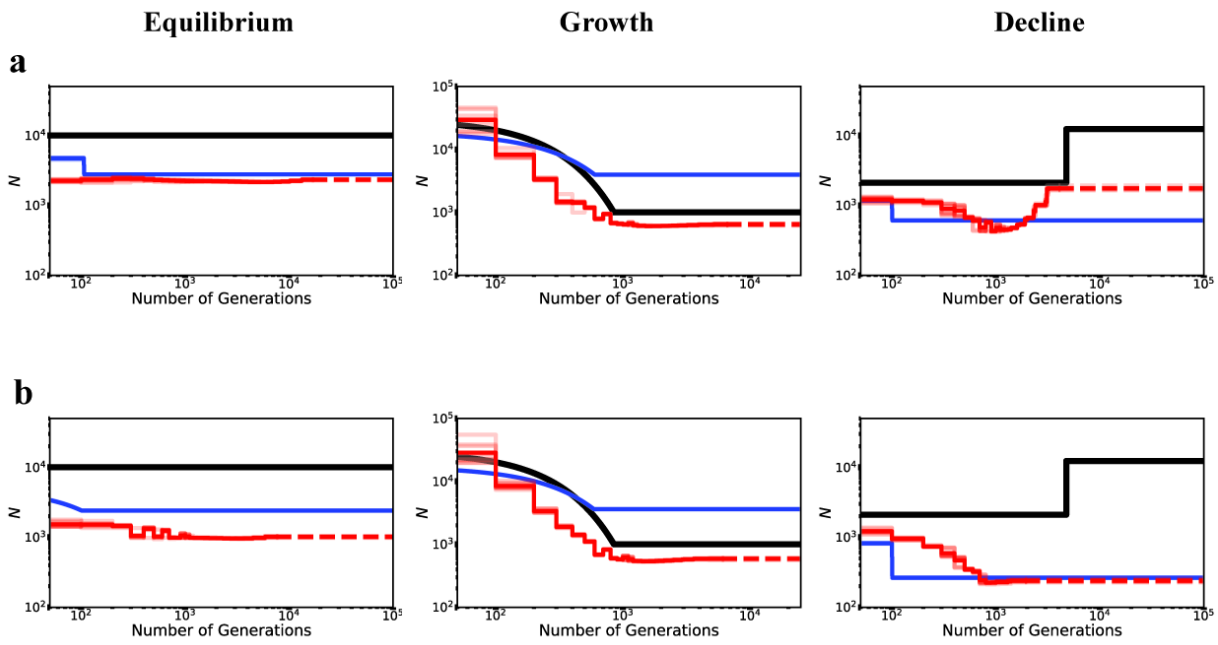

Figure 2: Inference of demography by MSMC (red lines; 10 replicates) and *fastsimcoal2* (blue lines; 10 replicates) in the presence of BGS generated by strongly deleterious mutations. Directly selected sites comprised 20% of the genome and were masked when performing demographic inference. (a) Exons experience purifying selection, with 30% of new mutations being strongly deleterious, and the remaining being neutral (specified by DFE6). (b) Exons experience purifying selection, with 50% of new mutations being strongly deleterious, and the remainder being neutral (specified by DFE5). The true demographic models are given as black lines, with the x-axis origin representing the present day. The dashed lines represent indefinite extensions of the ancestral population sizes.

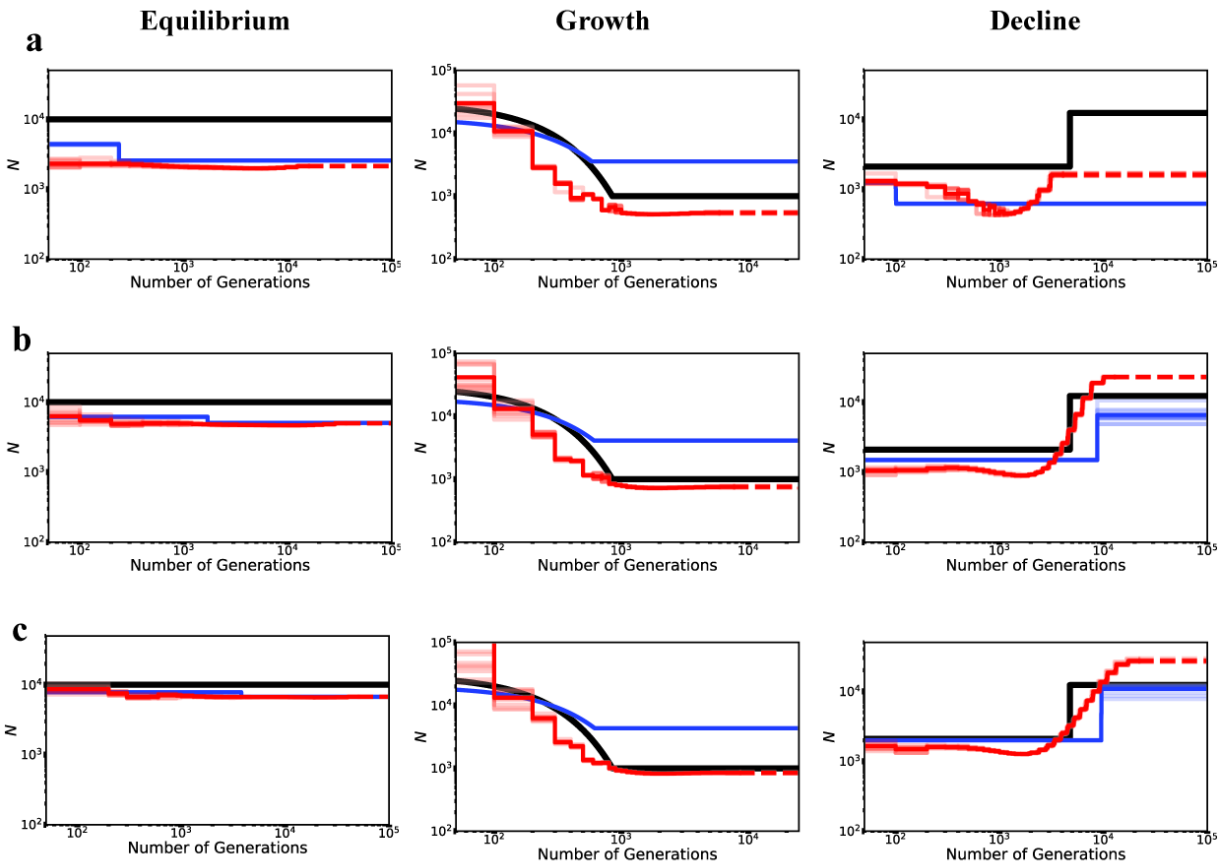

Figure 3: Inference of demography by MSMC (red lines; 10 replicates) and *fastsimcoal2* (blue lines; 10 replicates) in the presence of BGS with varying proportions of the genome under selection, for demographic equilibrium (left column), exponential growth (middle column), and instantaneous decline (right column). Exonic sites were simulated with purifying selection with all f_i values equal to 0.25 (DFE4), and were masked when performing inference. Directly selected sites comprise (a) 20% of the simulated genome, (b) 10% of the simulated genome, and (c) 5% of the simulated genome. The true demographic models are given by the black lines, with the x-axis origin representing the present day. The dashed lines represent indefinite extensions of the ancestral population sizes.

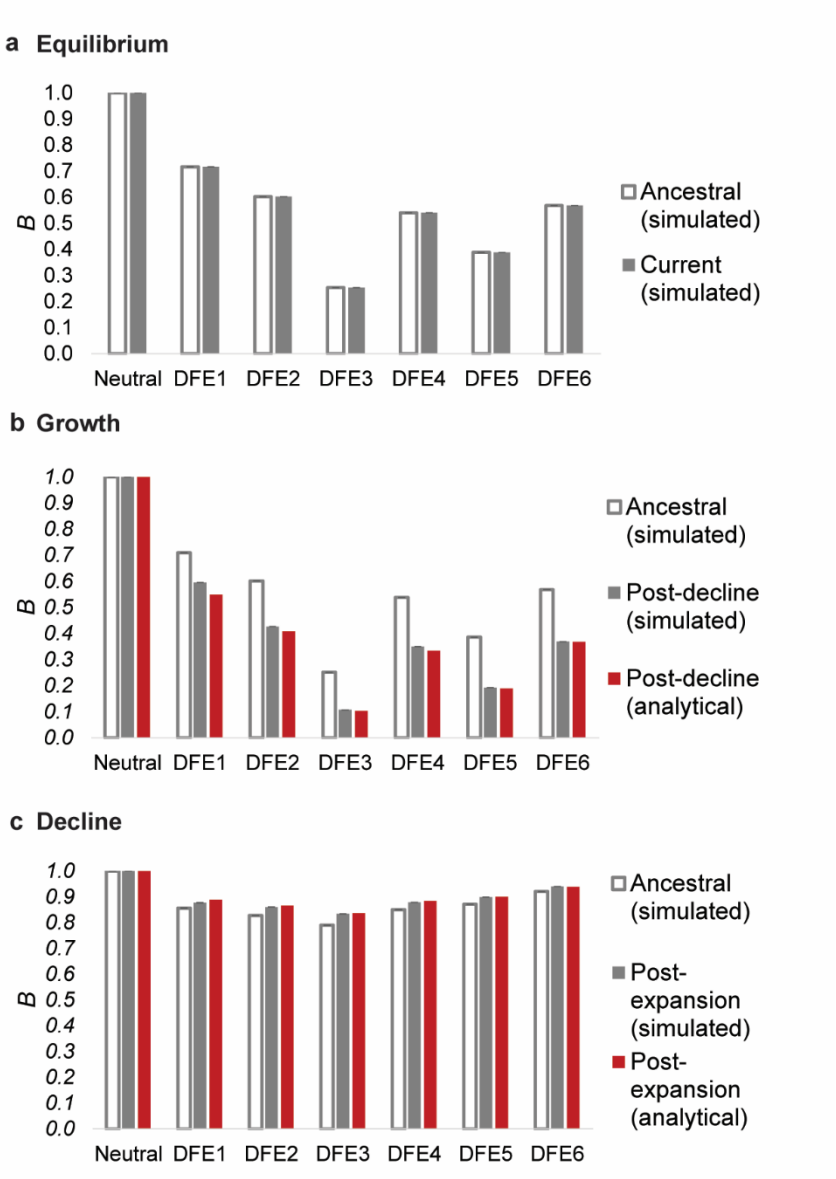

Figure 4: B is the nucleotide site diversity (π) with BGS relative to its purely neutral expectation (π_0). The results are shown for (a) demographic equilibrium, (b) population growth, and (c) population decline. For all cases, the ancestral B (*i.e.*, B pre-change in population size) is shown in white bars, B post-change in population size is shown in solid gray bars, and the analytical expectations for the post-size change B is shown as red bars. Various DFEs were used: **DFE1**: $f_0 = 0.1$, $f_1 = 0.7$, $f_2 = 0.1$, $f_3 = 0.1$. **DFE2**: $f_0 = 0.1$, $f_1 = 0.1$, $f_2 = 0.7$, $f_3 = 0.1$. **DFE3**: $f_0 = 0.1$, $f_1 = 0.1$, $f_2 = 0.1$, $f_3 = 0.7$. **DFE4**: $f_0 = f_1 = f_2 = f_3 = 0.25$. **DFE5:** $f_0 = 0.5$, $f_1 = 0.0$, $f_2 = 0.0$, $f_3 = 0.5$. **DFE6:** $f_0 = 0.7$, $f_1 = 0.0$, $f_2 = 0.0$, $f_3 = 0.3$. Exonic sites comprised ~10% of the genome, roughly mimicking the density of the human genome.

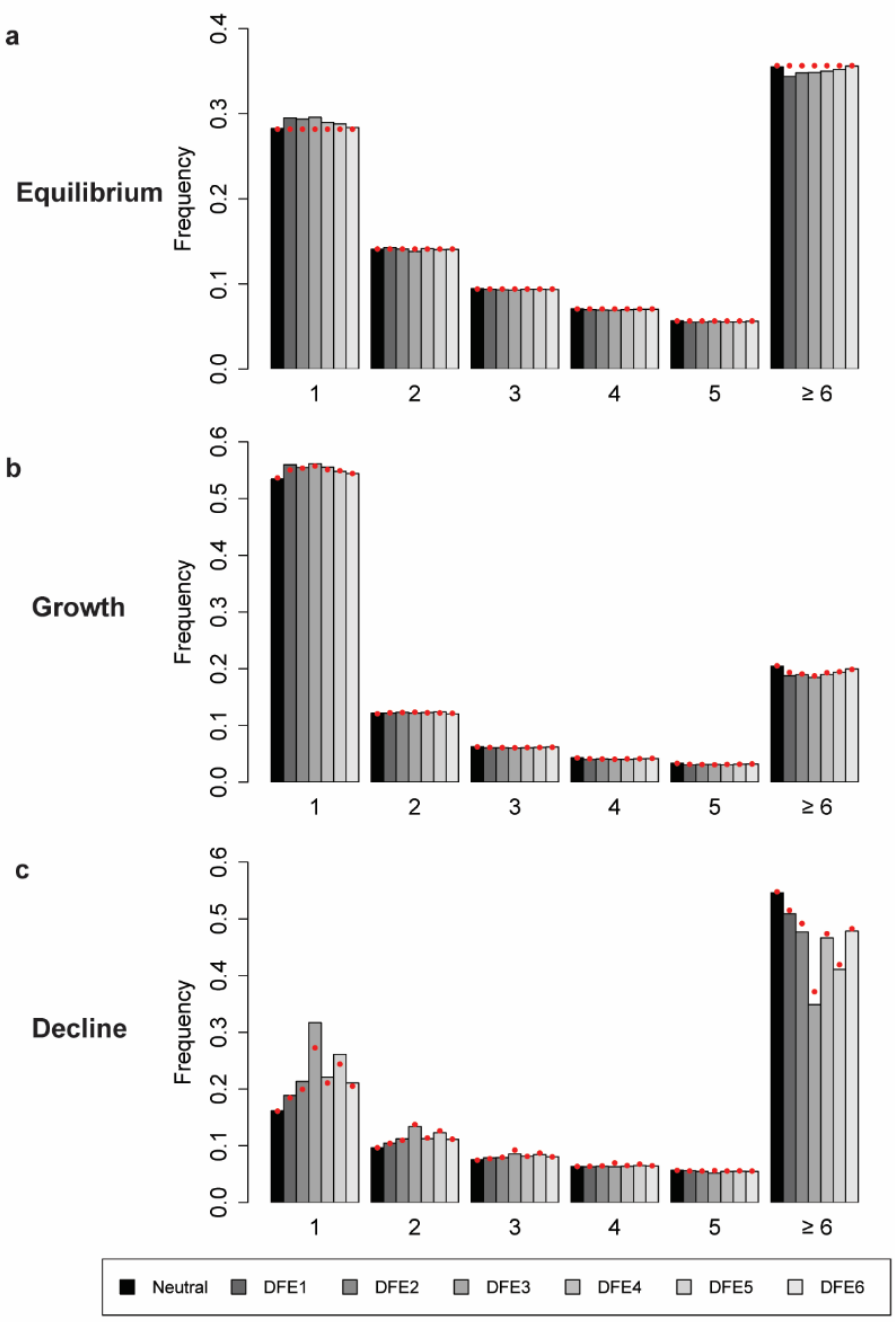

Figure 5: The site frequency spectrum (SFS) of derived allele frequencies at neutral sites from 10 diploid genomes under (a) demographic equilibrium, (b) population growth, and (c) population decline, under the same DFEs as shown in Figure 4. The x-axis indicates the number of sample alleles (out of 20) carrying the derived variant. Exonic sites comprised ~10% of the genome, roughly mimicking the density of the human genome. The red solid circles give the values predicted analytically with a purely neutral model, but taking the simulation values of B into account in order to quantify the effective population size.

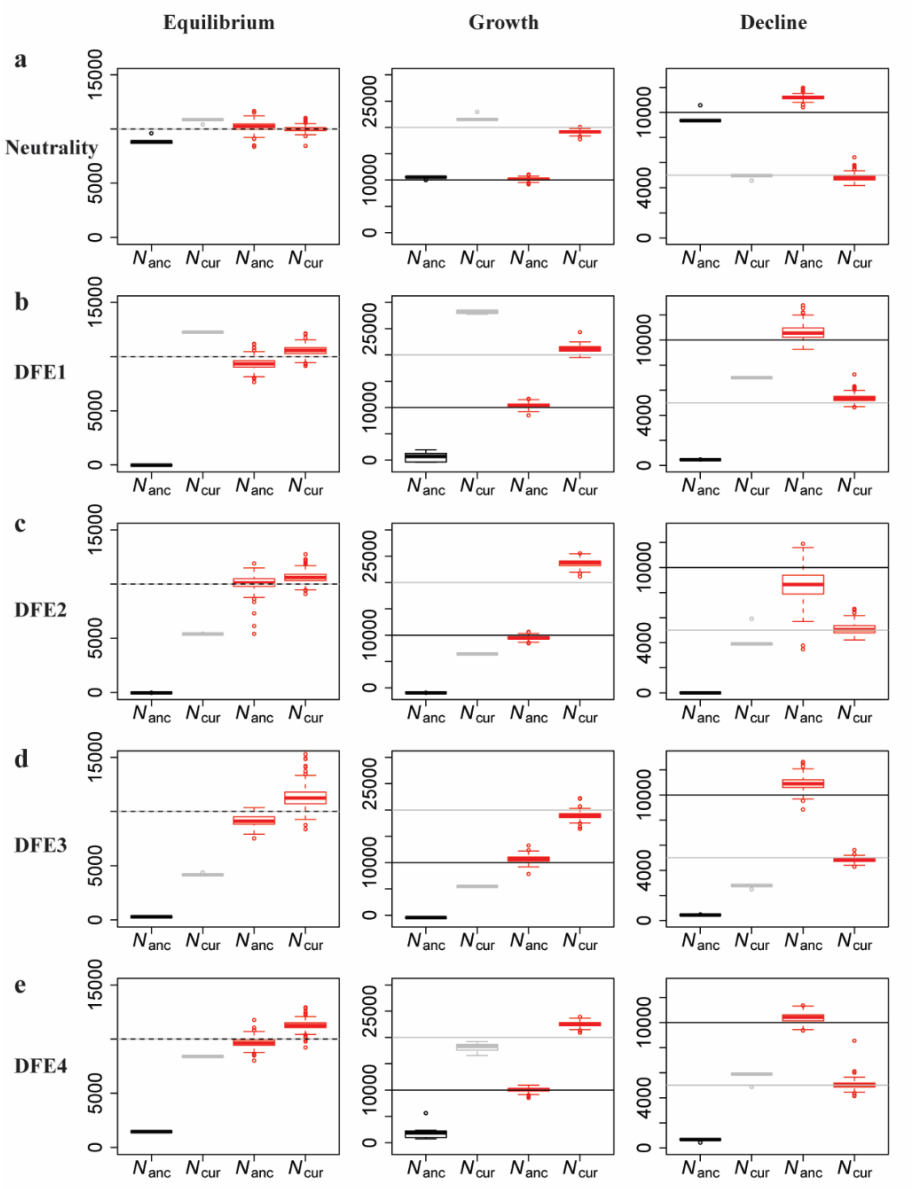

Figure 6: Comparison of estimates of ancestral (N_{anc}) and current (N_{cur}) population sizes when assuming neutrality *vs* when varying the DFE shape as a nuisance parameter, using an ABC framework. Inference is shown for demographic equilibrium (left column), 2-fold exponential growth (middle column), and 2-fold population decline (right column), for five separate DFE shapes that define the extent of direct purifying selection acting on the genomic segment for which demographic inference is performed: (a) neutrality ($f_0 = 1$, $f_1 = 0$, $f_2 = 0$, $f_3 = 0$), (b) weak purifying selection (DFE1: $f_0 = 0.1$, $f_1 = 0.7$, $f_2 = 0.1$, $f_3 = 0.1$), (c) moderately strong purifying selection (DFE2: $f_0 = 0.1$, $f_1 = 0.1$, $f_2 = 0.7$, $f_3 = 0.1$), (d) strong purifying selection (DFE3: $f_0 = 0.1$, $f_1 = 0.1$, $f_2 = 0.1$, $f_3 = 0.7$), and (e) a DFE in which all classes of mutations are equally frequent (DFE4: $f_0 = f_1 = f_2 = f_3 = 0.25$). In each, the horizontal lines give the true values (black for N_{anc}; and gray for N_{cur}) and the box-plots give the estimated values. Black and gray boxes represent estimates when assuming neutrality, while red boxes represent estimates when the DFE is treated as a nuisance parameter.

762 **REFERENCES**

763

764 Andolfatto P. 2005. Adaptive evolution of non-coding DNA in *Drosophila*. *Nature* 437:1149–
765 1152.

766 Bank C, Ewing GB, Ferrer-Admettla A, Foll M, Jensen JD. 2014. Thinking too positive?
767 Revisiting current methods of population genetic selection inference. *Trends Genet.*
768 30:540–546.

769 Beichman AC, Huerta-Sanchez E, Lohmueller KE. 2018. Using genomic data to infer historic
770 population dynamics of nonmodel organisms. *Annu. Rev. Ecol. Evol. Syst.* 49:433–456.

771 Beichman AC, Phung TN, Lohmueller KE. 2017. Comparison of single genome and allele
772 frequency data reveals discordant demographic histories. *G3* 7:3605–3620.

773 Bhaskar A, Wang YXR, Song YS. 2015. Efficient inference of population size histories and
774 locus-specific mutation rates from large-sample genomic variation data. *Genome Res.*
775 25:268–279.

776 Blattner FR, Plunkett G, Bloch CA, Perna NT, Burland V, Riley M, Collado-Vides J, Glasner
777 JD, Rode CK, Mayhew GF, et al. 1997. The complete genome sequence of *Escherichia*
778 *coli* K-12. *Science* 277:1453–1462.

779 Booker TR, Keightley PD. 2018. Understanding the factors that shape patterns of nucleotide
780 diversity in the house mouse genome. *Mol. Biol. Evol.* 35:2971–2988.

781 Bunnefeld L, Frantz LAF, Lohse K. 2015. Inferring bottlenecks from genome-wide samples of
782 short sequence blocks. *Genetics* 201:1157–1169.

783 Campos JL, Charlesworth B. 2019. The effects on neutral variability of recurrent selective
784 sweeps and background selection. *Genetics* 212:287–303.

785 Campos JL, Halligan DL, Haddrill PR, Charlesworth B. 2014. The relation between
786 recombination rate and patterns of molecular evolution and variation in *Drosophila*
787 *melanogaster*. *Mol. Biol. Evol.* 31:1010–1028.

788 Campos JL, Zhao L, Charlesworth B. 2017. Estimating the parameters of background selection
789 and selective sweeps in *Drosophila* in the presence of gene conversion. *Proc. Natl. Acad.*
790 *Sci. U.S.A.* 114:E4762–E4771.

791 Castellano D, Eyre-Walker A, Munch K. 2020. Impact of mutation rate and selection at linked
792 sites on DNA variation across the genomes of humans and other Homininae. *Genome*
793 *Biol. Evol.* 12:3550–3561.

794 Chamary J, Hurst LD. 2005. Evidence for selection on synonymous mutations affecting stability
795 of mRNA secondary structure in mammals. *Genome Biol.* 6:R75.

796 Charlesworth B. 2013. Background selection 20 years on. The Wilhelmine E. Key 2012
797 invitational lecture. *J. Hered.* 104:161–171.

798 Charlesworth B. 2015. Causes of natural variation in fitness: evidence from studies of
799 *Drosophila* populations. *Proc. Natl. Acad. Sci. U.S.A.* 112:1662–1669.

800 Charlesworth B, Morgan MT, Charlesworth D. 1993. The effect of deleterious mutations on
801 neutral molecular variation. *Genetics* 134:1289–1303.

802 Charlesworth D, Charlesworth B, Morgan MT. 1995. The pattern of neutral molecular variation
803 under the background selection model. *Genetics* 141:1619–1632.

804 Chikhi L, Rodríguez W, Grusea S, Santos P, Boitard S, Mazet O. 2018. The IICR (inverse
805 instantaneous coalescence rate) as a summary of genomic diversity: insights into
806 demographic inference and model choice. *Heredity* 120:13–24.

807 Choi JY, Aquadro CF. 2016. Recent and long term selection across synonymous sites in
808 *Drosophila ananassae*. *J. Mol. Evol.* 83:50–60.

809 Comeron JM, Kreitman M. 2002. Population, evolutionary and genomic consequences of
810 interference selection. *Genetics* 161:389–410.

811 Comeron JM, Ratnappan R, Bailin S. 2012. The many landscapes of recombination in
812 *Drosophila melanogaster*. *PLoS Genet.* 8:e1002905.

813 Csilléry K, Blum MGB, Gaggiotti OE, François O. 2010. Approximate Bayesian Computation
814 (ABC) in practice. *Trends Ecol. Evol.* 25:410–418.

815 Cutter AD, Payseur BA. 2013. Genomic signatures of selection at linked sites: unifying the
816 disparity among species. *Nat. Rev. Genet.* 14:262–274.

817 Elyashiv E, Sattath S, Hu TT, Strutsovsky A, McVicker G, Andolfatto P, Coop G, Sella G. 2016.
818 A genomic map of the effects of linked selection in *Drosophila*. *PLoS Genet.*
819 12:e1006130.

820 Ewing GB, Jensen JD. 2016. The consequences of not accounting for background selection in
821 demographic inference. *Mol. Ecol.* 25:135–141.

822 Excoffier L, Dupanloup I, Huerta-Sánchez E, Sousa VC, Foll M. 2013. Robust demographic
823 inference from genomic and SNP data. *PLoS Genet.* 9:e1003905.

824 Eyre-Walker A, Keightley PD. 2009. Estimating the rate of adaptive molecular evolution in the
825 presence of slightly deleterious mutations and population size change. *Mol. Biol. Evol.*
826 26:2097–2108.

827 Fay JC, Wu CI. 1999. A human population bottleneck can account for the discordance between
828 patterns of mitochondrial versus nuclear DNA variation. *Mol. Biol. Evol.* 16:1003–1005.

829 Fiston-Lavier A-S, Singh ND, Lipatov M, Petrov DA. 2010. *Drosophila melanogaster*
830 recombination rate calculator. *Gene* 463:18–20.

831 Francioli LC, Polak PP, Koren A, Menelaou A, Chun S, Renkens I, van Duijn CM, Swertz M,
832 Wijmenga C, van Ommen G, et al. 2015. Genome-wide patterns and properties of de
833 novo mutations in humans. *Nat Genet* 47:822–826.

834 Fulgione A, Koornneef M, Roux F, Hermisson J, Hancock AM. 2018. Madeiran Arabidopsis
835 thaliana reveals ancient long-range colonization and clarifies demography in Eurasia.
836 *Mol. Biol. Evol.* 35:564–574.

837 Gutenkunst RN, Hernandez RD, Williamson SH, Bustamante CD. 2009. Inferring the joint
838 demographic history of multiple populations from multidimensional SNP frequency data.
839 *PLoS Genet.* 5:e1000695.

840 Haddrill PR, Thornton KR, Charlesworth B, Andolfatto P. 2005. Multilocus patterns of
841 nucleotide variability and the demographic and selection history of *Drosophila*
842 *melanogaster* populations. *Genome Res.* 15:790–799.

843 Haller BC, Messer PW. 2019. SLiM 3: Forward genetic simulations beyond the Wright–Fisher
844 model. *Mol. Biol. Evol.* 36:632–637.

845 Harris K, Nielsen R. 2013. Inferring demographic history from a spectrum of shared haplotype
846 lengths. *PLoS Genet.* 9:e1003521.

847 Hernandez RD, Kelley JL, Elyashiv E, Melton SC, Auton A, McVean G, Project 1000 Genomes,
848 Sella G, Przeworski M. 2011. Classic selective sweeps were rare in recent human
849 evolution. *Science* 331:920–924.

850 Hey J, Harris E. 1999. Population bottlenecks and patterns of human polymorphism. *Mol Biol*
851 *Evol* 16:1423–1426.

852 Hill WG, Robertson A. 1966. The effect of linkage on limits to artificial selection. *Genet. Res.*
853 8:269–294.

854 Hoggart CJ, Chadeau-Hyam M, Clark TG, Lampariello R, Whittaker JC, Iorio MD, Balding DJ.
855 2007. Sequence-level population simulations over large genomic regions. *Genetics*
856 177:1725–1731.

857 Hung C-M, Shaner P-JL, Zink RM, Liu W-C, Chu T-C, Huang W-S, Li S-H. 2014. Drastic
858 population fluctuations explain the rapid extinction of the passenger pigeon. *Proc. Nat.*
859 *Acad. Sci. U.S.A.* 111:10636–10641.

860 Jackson BC, Campos JL, Haddrill PR, Charlesworth B, Zeng K. 2017. Variation in the intensity
861 of selection on codon bias over time causes contrasting patterns of base composition
862 evolution in *Drosophila*. *Genome Biol. Evol.* 9:102–123.

863 Jacquier H, Birgy A, Nagard HL, Mechulam Y, Schmitt E, Glodt J, Bercot B, Petit E, Poulain J,
864 Barnaud G, et al. 2013. Capturing the mutational landscape of the beta-lactamase TEM-1.
865 *Proc. Natl. Acad. Sci. U.S.A.* 110:13067–13072.

866 Jensen JD, Payseur BA, Stephan W, Aquadro CF, Lynch M, Charlesworth D, Charlesworth B.
867 2019. The importance of the Neutral Theory in 1968 and 50 years on: A response to Kern
868 and Hahn 2018. *Evolution* 73:111–114.

869 Johri P, Charlesworth B, Jensen JD. 2020. Toward an evolutionarily appropriate null model:
870 jointly inferring demography and purifying selection. *Genetics* 215:173–192.

871 Jones MR, Good JM. 2016. Targeted capture in evolutionary and ecological genomics. *Mol.*
872 *Ecol.* 25:185–202.

873 Kaiser VB, Charlesworth B. 2009. The effects of deleterious mutations on evolution in non-
874 recombining genomes. *Trends Genet.* 25:9–12.

875 Keightley PD, Eyre-Walker A. 2007. Joint inference of the distribution of fitness effects of
876 deleterious mutations and population demography based on nucleotide polymorphism
877 frequencies. *Genetics* 177:2251–2261.

878 Keightley PD, Jackson BC. 2018. Inferring the probability of the derived vs. the ancestral allelic
879 state at a polymorphic site. *Genetics* 209:897–906.

880 Keightley PD, Ness RW, Halligan DL, Haddrill PR. 2014. Estimation of the spontaneous
881 mutation rate per nucleotide site in a *Drosophila melanogaster* full-sib family. *Genetics*
882 196:313–320.

883 Keightley PD, Trivedi U, Thomson M, Oliver F, Kumar S, Blaxter ML. 2009. Analysis of the
884 genome sequences of three *Drosophila melanogaster* spontaneous mutation accumulation
885 lines. *Genome Res.* 19:1195–1201.

886 Kelleher J, Wong Y, Wohns AW, Fadil C, Albers PK, McVean G. 2019. Inferring whole-
887 genome histories in large population datasets. *Nat. Genet.* 51:1330–1338.

888 Kent WJ, Sugnet CW, Furey TS, Roskin KM, Pringle TH, Zahler AM, Haussler and D. 2002.
889 The Human Genome Browser at UCSC. *Genome Res.* 12:996–1006.

890 Kim Y, Wiehe T. 2009. Simulation of DNA sequence evolution under models of recent
891 directional selection. *Brief. Bioinformatics* 10:84–96.

892 Kousathanas A, Keightley PD. 2013. A comparison of models to infer the distribution of fitness
893 effects of new mutations. *Genetics* 193:1197–1208.

894 Lander ES, Linton LM, Birren B, Nusbaum C, Zody MC, Baldwin J, Devon K, Dewar K, Doyle
895 M, FitzHugh W, et al. 2001. Initial sequencing and analysis of the human genome.
896 *Nature* 409:860–921.

897 Lapierre M, Lambert A, Achaz G. 2017. Accuracy of demographic inferences from the site
898 frequency spectrum: the case of the Yoruba population. *Genetics* 206:439–449.

899 Li H, Durbin R. 2011. Inference of human population history from individual whole-genome
900 sequences. *Nature* 475:493–496.

901 Liang P, Saqib HSA, Zhang X, Zhang L, Tang H. 2018. Single-base resolution map of
902 evolutionary constraints and annotation of conserved elements across major grass
903 genomes. *Genome Biol. Evol.* 10:473–488.

904 Lukic S, Hey J. 2012. Demographic inference using spectral methods on SNP data, with an
905 analysis of the human out-of-Africa expansion. *Genetics* 192:619–639.

906 Lynch M. 2007. The Origins of Genome Architecture. illustrated ed. Sunderland, Massachusetts:
907 Sinauer Associates

908 Mazet O, Rodríguez W, Grusea S, Boitard S, Chikhi L. 2016. On the importance of being
909 structured: instantaneous coalescence rates and human evolution--lessons for ancestral
910 population size inference? *Heredity* 116:362–371.

911 Messer PW, Petrov DA. 2013. Frequent adaptation and the McDonald–Kreitman test. *Proc. Natl.*
912 *Acad. Sci. U.S.A.* 110:8615–8620.

913 Nicolaisen LE, Desai MM. 2013. Distortions in genealogies due to purifying selection and
914 recombination. *Genetics* 195:221–230.

915 O'Fallon BD, Seger J, Adler FR. 2010. A continuous-state coalescent and the impact of weak
916 selection on the structure of gene genealogies. *Mol. Biol. Evol.* 27:1162–1172.

917 Orozco-terWengel P. 2016. The devil is in the details: the effect of population structure on
918 demographic inference. *Heredity* 116:349–350.

919 Palkopoulou E, Lipson M, Mallick S, Nielsen S, Rohland N, Baleka S, Karpinski E, Ivancevic
920 AM, To T-H, Kortschak RD, et al. 2018. A comprehensive genomic history of extinct
921 and living elephants. *Proc. Nat. Acad. Sci. U.S.A.* 115:E2566–E2574.

922 Polanski A, Bobrowski A, Kimmel M. 2003. A note on distributions of times to coalescence,
923 under time-dependent population size. *Theor Popul Biol* 63:33–40.

924 Polanski A, Kimmel M. 2003. New explicit expressions for relative frequencies of single-
925 nucleotide polymorphisms with application to statistical inference on population growth.
926 *Genetics* 165:427–436.

927 Pool JE, Nielsen R. 2007. Population size changes reshape genomic patterns of diversity.
928 *Evolution* 61:3001–3006.

929 Pool JE, Nielsen R. 2009. Correction for Pool and Nielsen (2007). *Evolution* 63:1671.

930 Pouyet F, Aeschbacher S, Thiéry A, Excoffier L. 2018. Background selection and biased gene
931 conversion affect more than 95% of the human genome and bias demographic
932 inferences.Veeramah K, Wittkopp PJ, Gronau I, editors. *eLife* 7:e36317.

933 Ragsdale AP, Gutenkunst RN. 2017. Inferring demographic history using two-locus statistics.
934 *Genetics* 206:1037–1048.

935 Sanjuán R. 2010. Mutational fitness effects in RNA and single-stranded DNA viruses: common
936 patterns revealed by site-directed mutagenesis studies. *Philos. Trans. R. Soc. Lond., B,*
937 *Biol. Sci.* 365:1975–1982.

938 Schiffels S, Durbin R. 2014. Inferring human population size and separation history from
939 multiple genome sequences. *Nat. Genet.* 46:919–925.

940 Schneider A, Charlesworth B, Eyre-Walker A, Keightley PD. 2011. A method for inferring the
941 rate of occurrence and fitness effects of advantageous mutations. *Genetics* 189:1427–
942 1437.

943 Schrider DR, Shanku AG, Kern AD. 2016. Effects of linked selective sweeps on demographic
944 inference and model selection. *Genetics* 204:1207–1223.

945 Sheehan S, Song YS. 2016. Deep learning for population genetic inference. *PLoS Comput. Biol.*
946 12:e1004845.

947 Siepel A, Bejerano G, Pedersen JS, Hinrichs AS, Hou M, Rosenbloom K, Clawson H, Spieth J,
948 Hillier LW, Richards S, et al. 2005. Evolutionarily conserved elements in vertebrate,
949 insect, worm, and yeast genomes. *Genome Res.* 15:1034–1050.

950 Slatkin M, Hudson RR. 1991. Pairwise comparisons of mitochondrial DNA sequences in stable
951 and exponentially growing populations. *Genetics* 129:555–562.

952 Speidel L, Forest M, Shi S, Myers SR. 2019. A method for genome-wide genealogy estimation
953 for thousands of samples. *Nat. Genet.* 51:1321–1329.

954 Steinrücken M, Kamm J, Spence JP, Song YS. 2019. Inference of complex population histories
955 using whole-genome sequences from multiple populations. *Proc. Natl. Acad. Sci. U.S.A.*
956 116:17115–17120.

957 Teshima KM, Coop G, Przeworski M. 2006. How reliable are empirical genomic scans for
958 selective sweeps? *Genome Res* 16:702–712.

959 Thornton K. 2003. Libsequence: a C++ class library for evolutionary genetic analysis.
960 *Bioinformatics* 19:2325–2327.

961 Thornton KR, Jensen JD. 2007. Controlling the false-positive rate in multilocus genome scans
962 for selection. *Genetics* 175:737–750.

963 Torres R, Stetter MG, Hernandez RD, Ross-Ibarra J. 2020. The temporal dynamics of
964 background selection in nonequilibrium populations. *Genetics* 214:1019–1030.

965 Torres R, Szpiech ZA, Hernandez RD. 2018. Human demographic history has amplified the
966 effects of background selection across the genome. *PLoS Genet.* 14:e1007387.

967 Uricchio LH, Hernandez RD. 2014. Robust forward simulations of recurrent hitchhiking.
968 *Genetics* 197:221–236.

969 Warren WC, Jasinska AJ, García-Pérez R, Svardal H, Tomlinson C, Rocchi M, Archidiacono N,
970 Capozzi O, Minx P, Montague MJ, et al. 2015. The genome of the vervet (*Chlorocebus*
971 *aethiops sabaeus*). *Genome Res.* 25:1921–1933.

972 Williamson RJ, Josephs EB, Platts AE, Hazzouri KM, Haudry A, Blanchette M, Wright SI.
973 2014. Evidence for widespread positive and negative selection in coding and conserved
974 noncoding regions of *Capsella grandiflora*. *PLoS Genet.* 10:e1004622.

975 Wu F, Zhao S, Yu B, Chen Y-M, Wang W, Song Z-G, Hu Y, Tao Z-W, Tian J-H, Pei Y-Y, et al.
976 2020. A new coronavirus associated with human respiratory disease in China. *Nature*
977 579:265–269.

978 Zeng K, Charlesworth B. 2010. Studying patterns of recent evolution at synonymous sites and
979 intronic sites in *Drosophila melanogaster*. *J. Mol. Evol.* 70:116–128.

980 Zhou Y, Massonnet M, Sanjak JS, Cantu D, Gaut BS. 2017. Evolutionary genomics of grape
981 (*Vitis vinifera ssp. vinifera*) domestication. *Proc. Nat. Acad. Sci. U.S.A.* 114:11715–
982 11720.

983
984
985

SUPPLEMENTARY

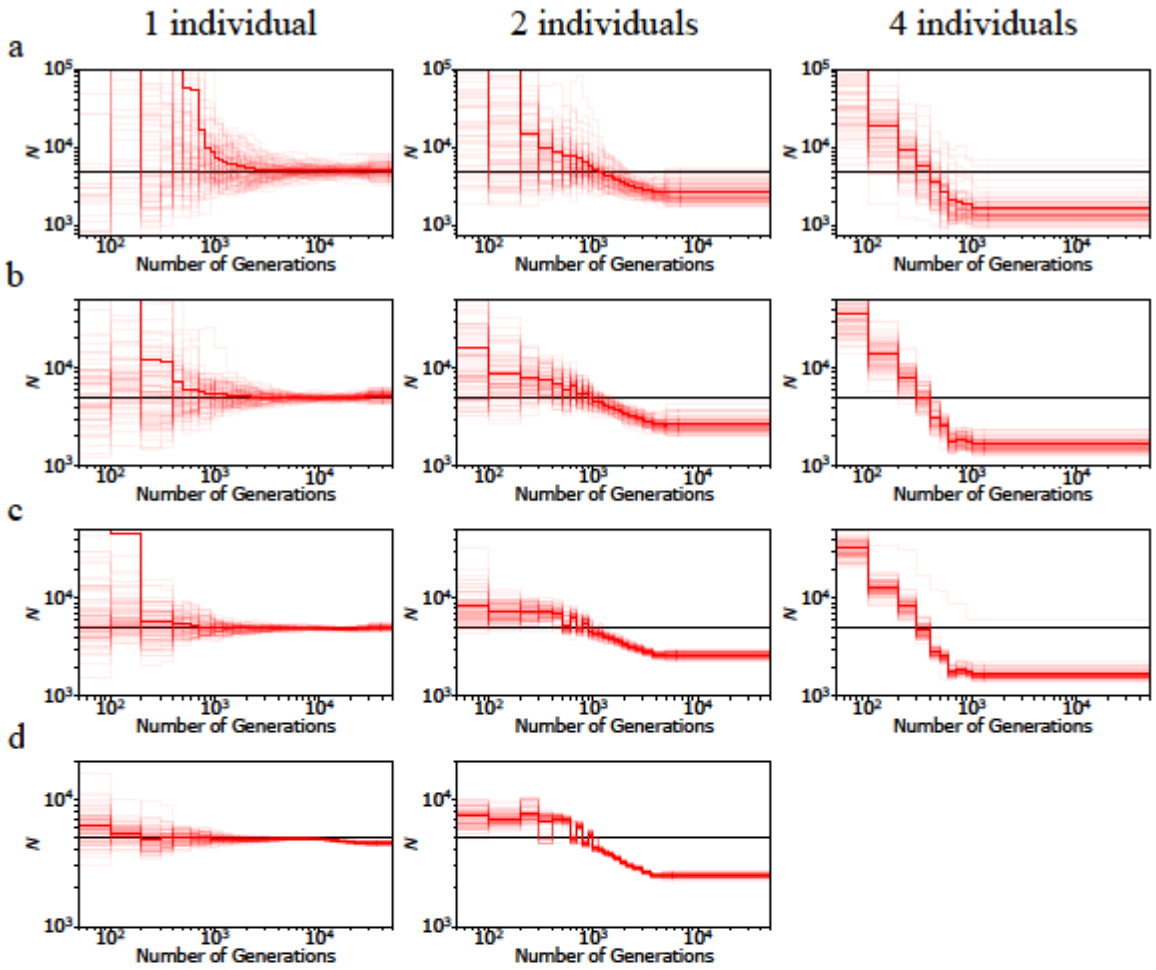

Supp Figure 1: Performance of MSMC under neutrality and demographic equilibrium when using 1, 2 and 4 diploid individuals for inference and with varying chromosome sizes: (a) 10 Mb, (b) 50 Mb, (c) 200 Mb, (d) 1 Gb. The numbers of replicates for each panel varied slightly around 100. MSMC runs with 4 diploid individuals could not be obtained due to the long computational times required. As shown, MSMC has a tendency to take a common shape, often falsely indicating recent population growth.

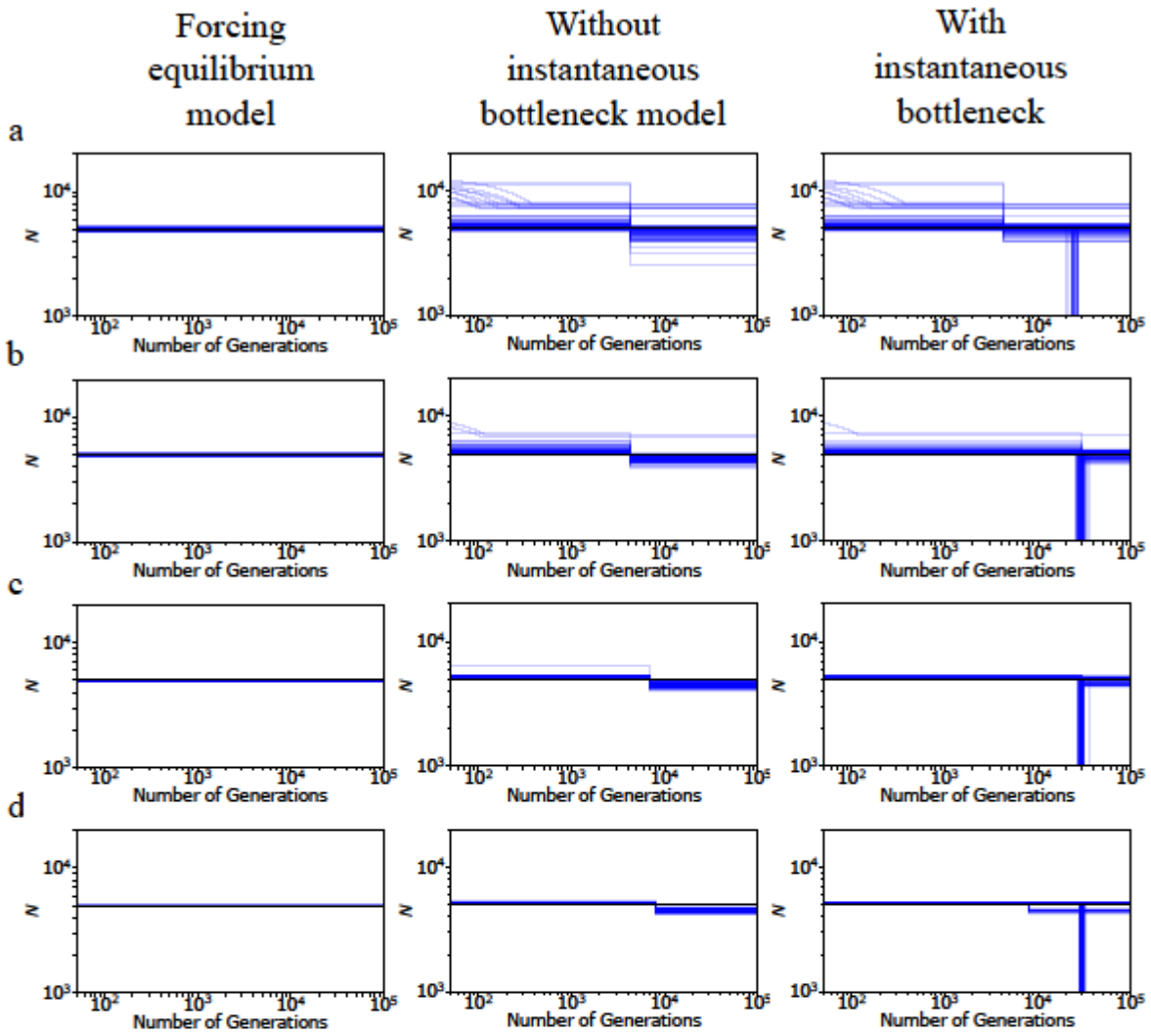

Supp Figure 2: Performance of *fastsimcoal2* under neutrality and demographic equilibrium with varying chromosome sizes: (a) 10 Mb, (b) 50 Mb, (c) 200 Mb, (d) 1 Gb and when different model choices are provided: *Left panel*: the correct model of constant population size is specified; *Middle panel*: model selection was performed between 3 models – equilibrium, instantaneous size change, and exponential size change; *Right panel*: model selection was performed between 4 models – equilibrium, instantaneous size change, exponential size change, and instantaneous bottleneck. Inference was performed using 50 diploid individuals and the inferred population size estimates of the best model are plotted (blue lines). The numbers of replicates for each panel varied slightly around 100. The true model is shown in black.

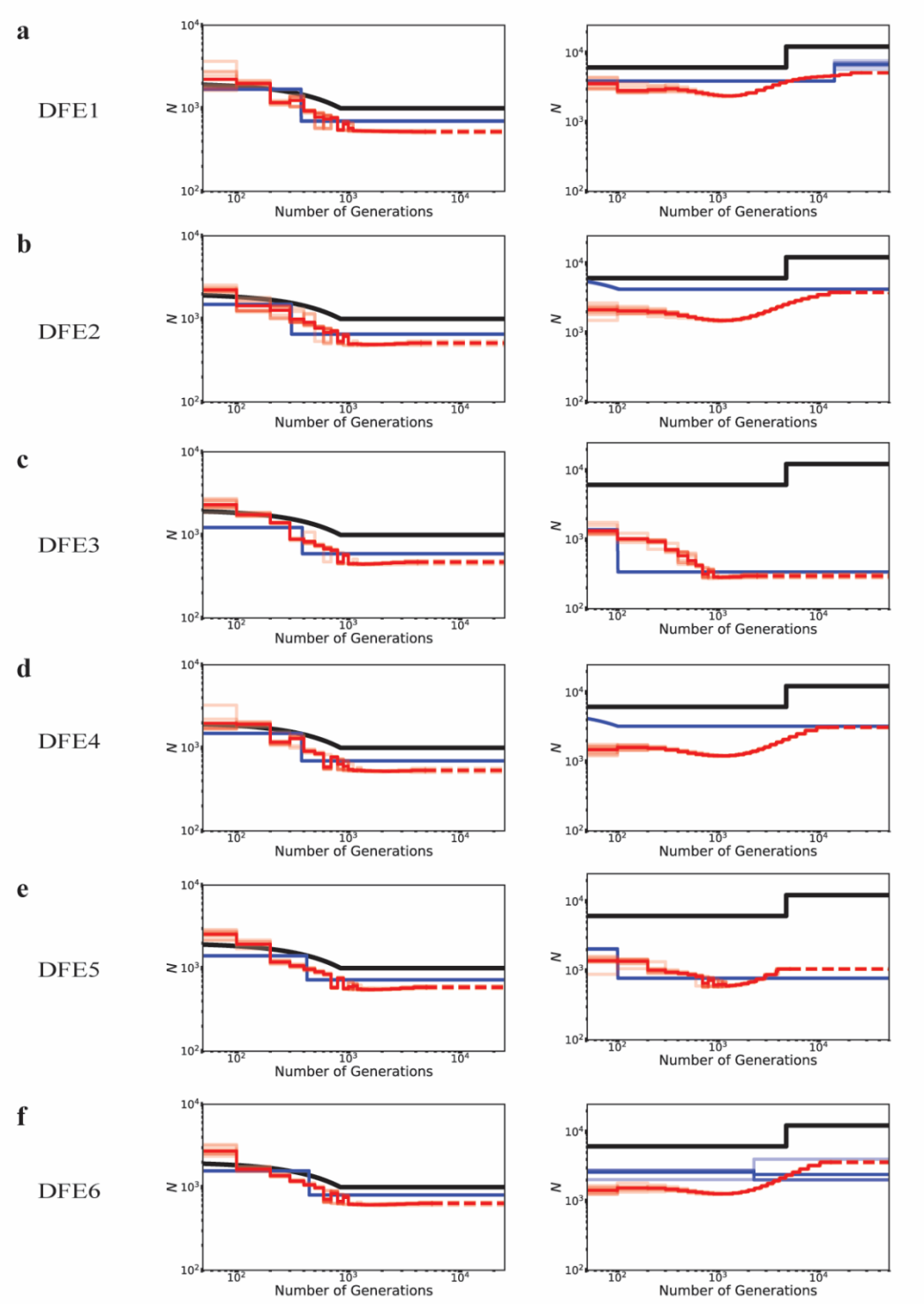

Supp Figure 3: Inferred demography from MSMC (red lines) and *fastsimcoal2* (blue lines) in the presence of background selection, with the true DFE shown to the left of the panel, for 2-fold instantaneous decline (right column) and 2-fold exponential growth (left column). In this case, 20% of the genome experiences direct selection. The true demographic models are shown as black lines.

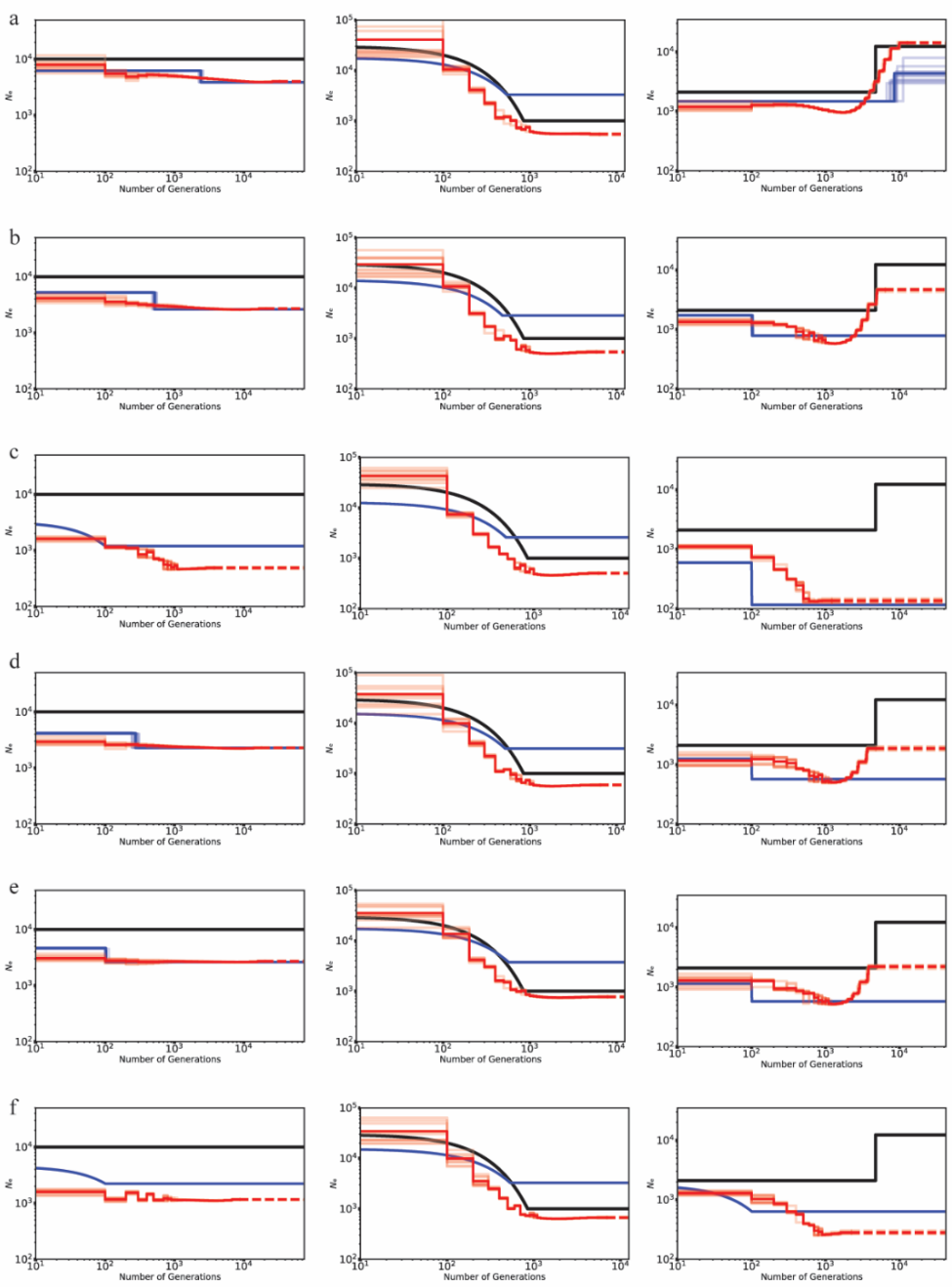

Supp Figure 4: Inference of demography by MSMC (red lines; 10 replicates) and *fastsimcoal2* (blue lines; 10 replicates) under demographic equilibrium (left column), 30-fold exponential growth (middle column), and ~6-fold instantaneous decline (right column) in the presence of direct purifying selection (*i.e.*, directly selected sites are not masked). The true demographic model is depicted in black lines. Exonic sites experience purifying selection specified by the following DFEs: (a) DFE1: $f_0 = 0.1$, $f_1 = 0.7$, $f_2 = 0.1$, $f_3 = 0.1$, (b) DFE2: $f_0 = 0.1$, $f_1 = 0.1$, $f_2 = 0.7$, $f_3 = 0.1$, (c) DFE3: $f_0 = 0.1$, $f_1 = 0.1$, $f_2 = 0.1$, $f_3 = 0.7$, (d) DFE4: $f_0 = 0.25$, $f_1 = 0.25$, $f_2 = 0.25$, $f_3 = 0.25$, (e) DFE5: $f_0 = 0.7$, $f_1 = 0.0$, $f_2 = 0.0$, $f_3 = 0.3$, (f) DFE6: $f_0 = 0.5$, $f_1 = 0.0$, $f_2 = 0.0$, $f_3 = 0.5$. In this case, 20% of the genome is under selection.

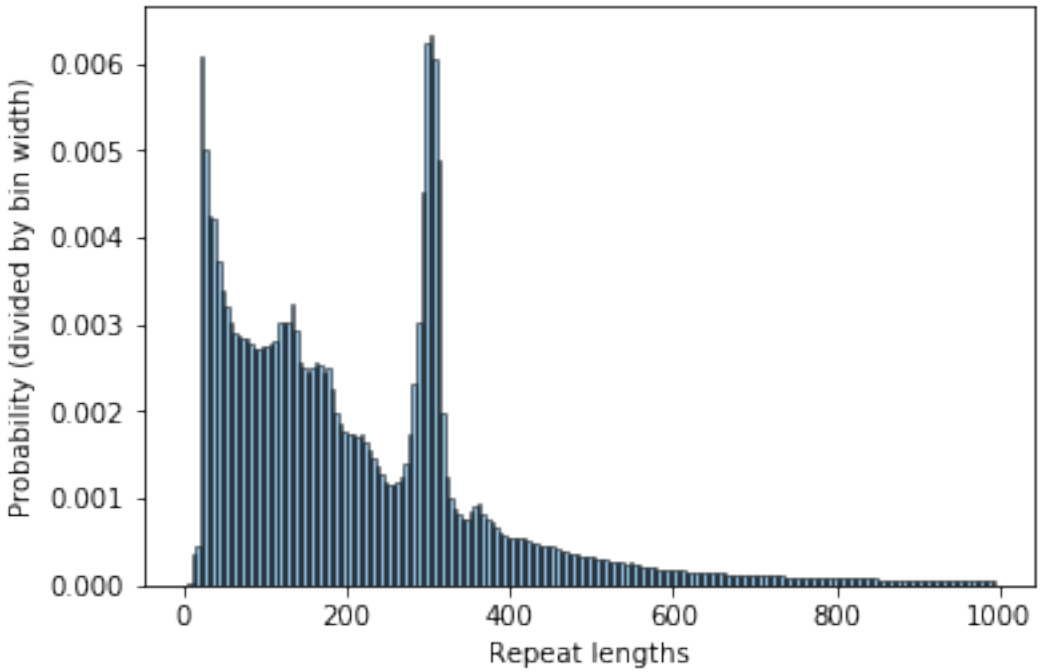

Supp Figure 5: Distribution of lengths of repeat regions in the human genomes (*hg19*). Shown above is the distribution of lengths up to 1000 bp, although lengths of repeat regions range between 6 to 160602 bp.

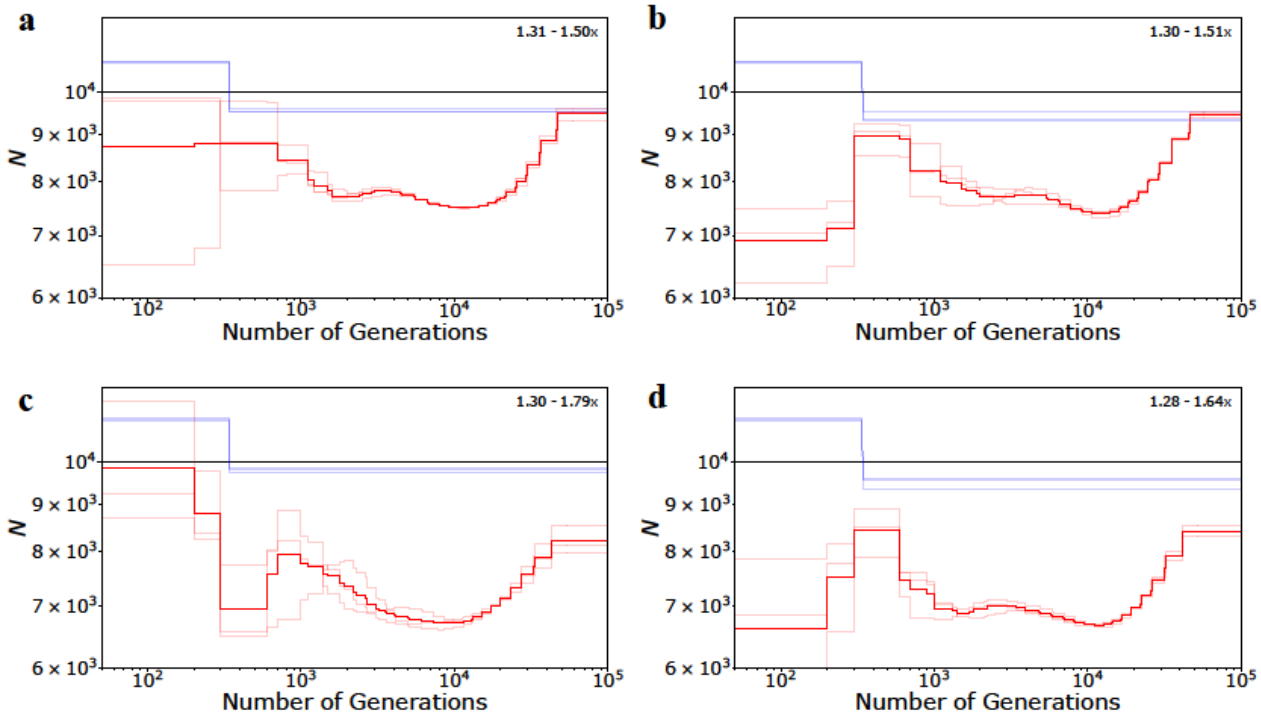

Supplementary Figure 6: Performance of demographic inference by MSMC (red lines) and *fastsimcoal2* (blue lines) under different scenarios of neutrality when the true model is equilibrium: (a) there is variation in recombination and mutation rates, (b) there is variation in recombination and mutation rates and the centromeric region is masked, (c) there is variation in recombination and mutation rates, and short regions resembling repeats (comprising 10% of each chromosome) are randomly masked across the genome, and (d) there is variation in recombination and mutation rates, and the centromere as well as small-sized repeats are randomly masked across the genome. The maximum and minimum fold change detected in every scenario is indicated on the upper right corner.

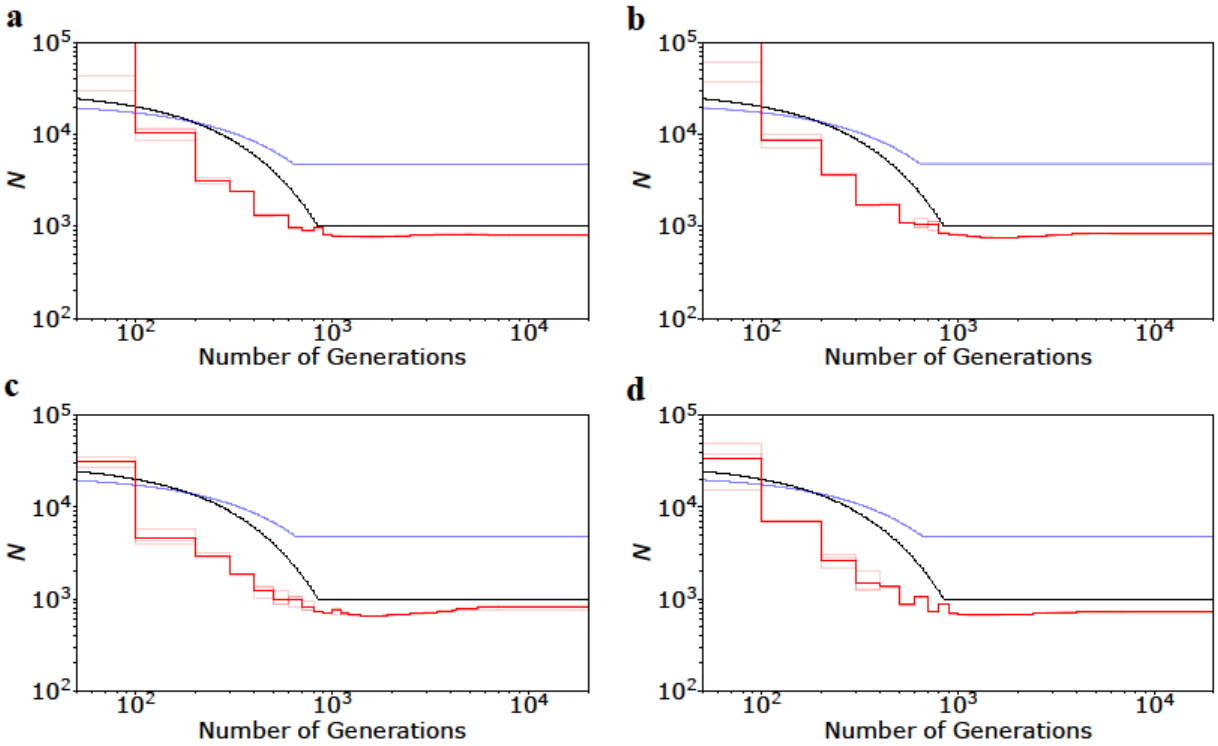

Supplementary Figure 7 : Performance of demographic inference by MSMC (red lines) and *fastsimcoal2* (blue lines) under different scenarios of neutrality when the true model is 30-fold exponential growth: (a) there is variation in recombination and mutation rates across the genome, (b) there is variation in recombination and mutation rates, and the centromeric region is masked, (c) there is variation in recombination and mutation rates, and short regions resembling repeats are randomly masked across the genome (comprising of 10% of each chromosome), and (d) there is variation in recombination and mutation rates, and the centromere as well as small-sized repeats are randomly masked across the genome.

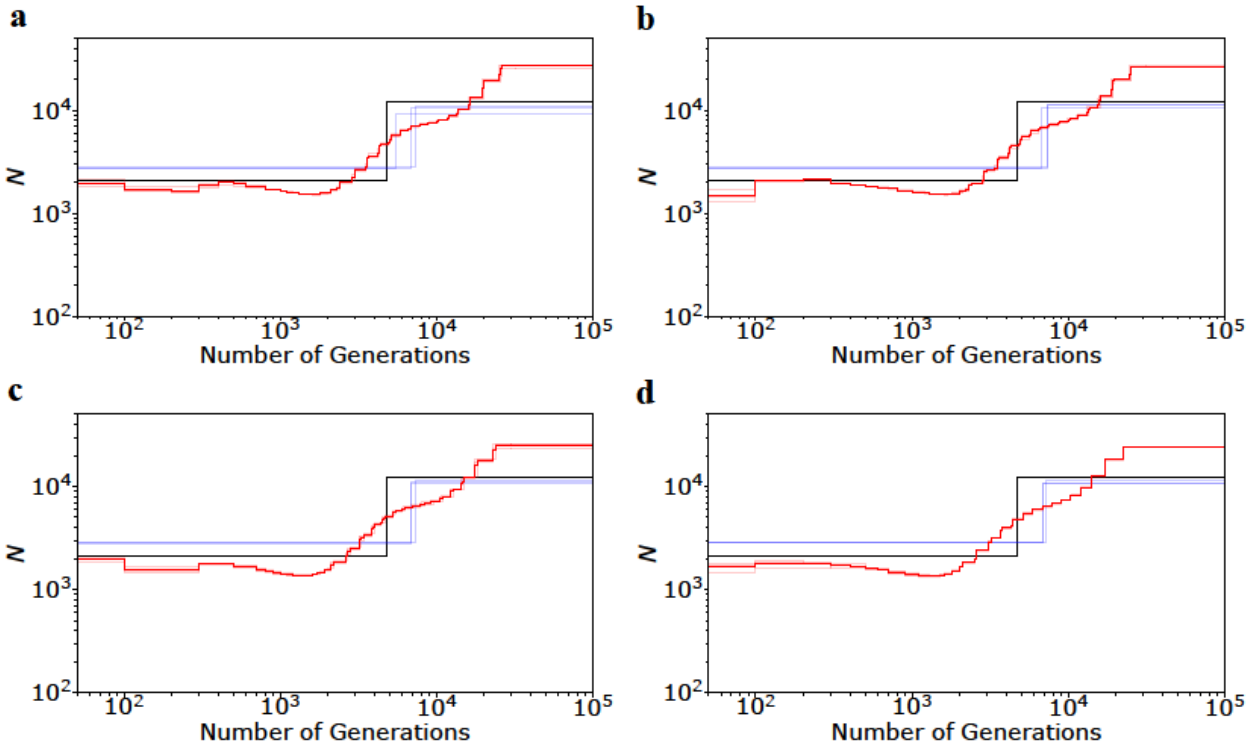

Supplementary Figure 8: Performance of demographic inference by MSMC under different scenarios of neutrality when the true model is 6-fold instantaneous decline: (a) there is variation in recombination and mutation rates across the genome, (b) there is variation in recombination and mutation rates, and the centromeric region is masked, (c) there is variation in recombination sand mutation rates, and short regions resembling repeats are randomly masked across the genome (comprising of 10% of each chromosome), and (d) there is variation in recombination and mutation rates, and the centromere as well as small-sized repeats are randomly masked across the genome.

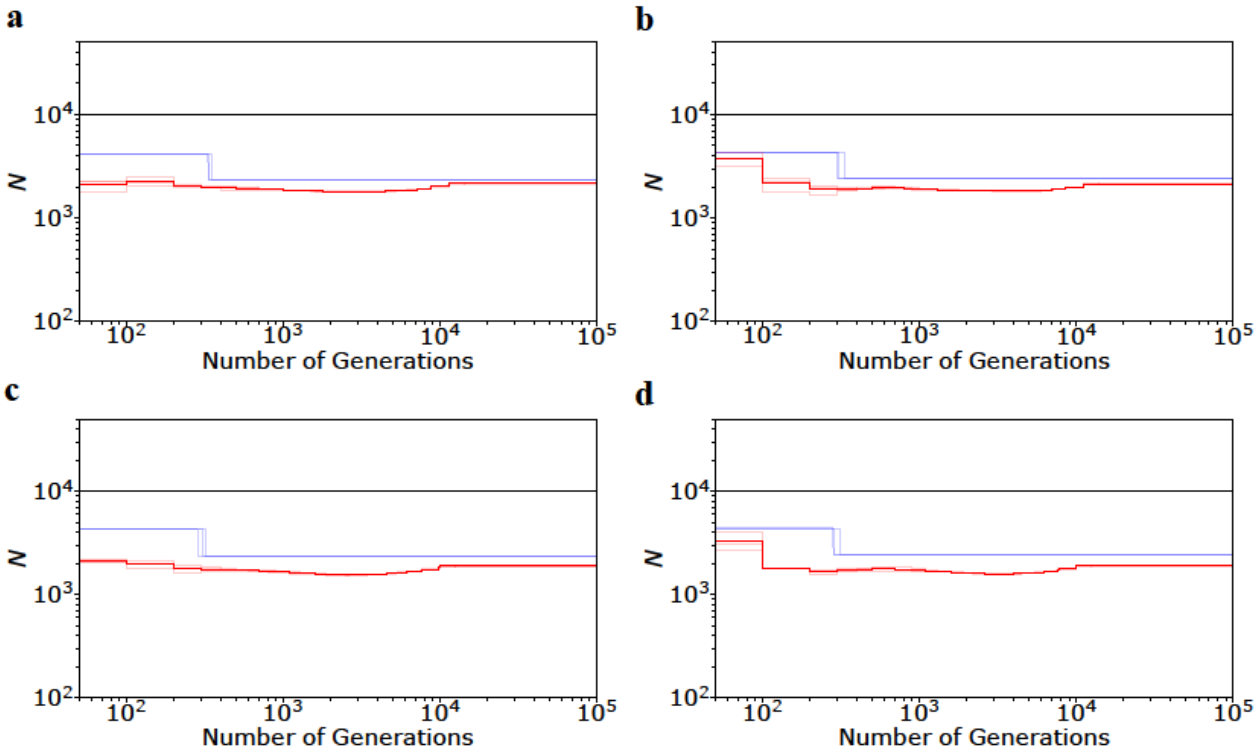

Supplementary Figure 9: Performance of demographic inference by MSMC (red lines) and *fastsimcoal2* (blue lines) in the presence of background selection, under different scenarios when the true model is equilibrium: (a) there is variation in recombination and mutation rates, (b) there is variation in recombination and mutation rates and the centromeric region is masked, (c) there is variation in recombination and mutation rates, and short regions resembling repeats (comprising 10% of each chromosome) are randomly masked across the genome, and (d) there is variation in recombination and mutation rates, and the centromere as well as small-sized repeats are randomly masked across the genome. Exons comprise of 20% of the genome, experience purifying selection given by DFE4 ($f_0 = f_1 = f_2 = f_3 = 0.25$) and are masked when performing inference.

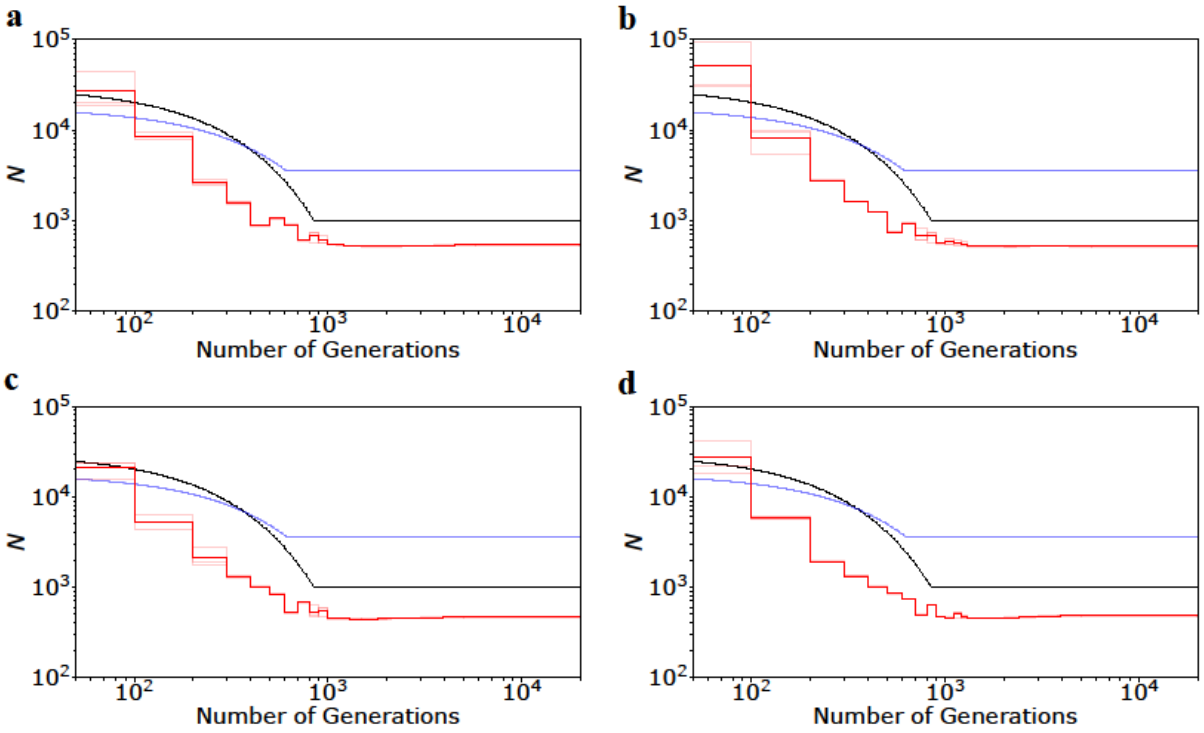

Supplementary Figure 10: Performance of demographic inference by MSMC (red lines) and *fastsimcoal2* (blue lines) in the presence of background selection, under different scenarios when the true model is 30-fold exponential growth: (a) there is variation in recombination and mutation rates, (b) there is variation in recombination and mutation rates and the centromeric region is masked, (c) there is variation in recombination and mutation rates, and short regions resembling repeats (comprising 10% of each chromosome) are randomly masked across the genome, and (d) there is variation in recombination and mutation rates, and the centromere as well as small-sized repeats are randomly masked across the genome. Exons comprise of 20% of the genome, experience purifying selection given by DFE4 ($f_0 = f_1 = f_2 = f_3 = 0.25$), and are masked when performing inference.

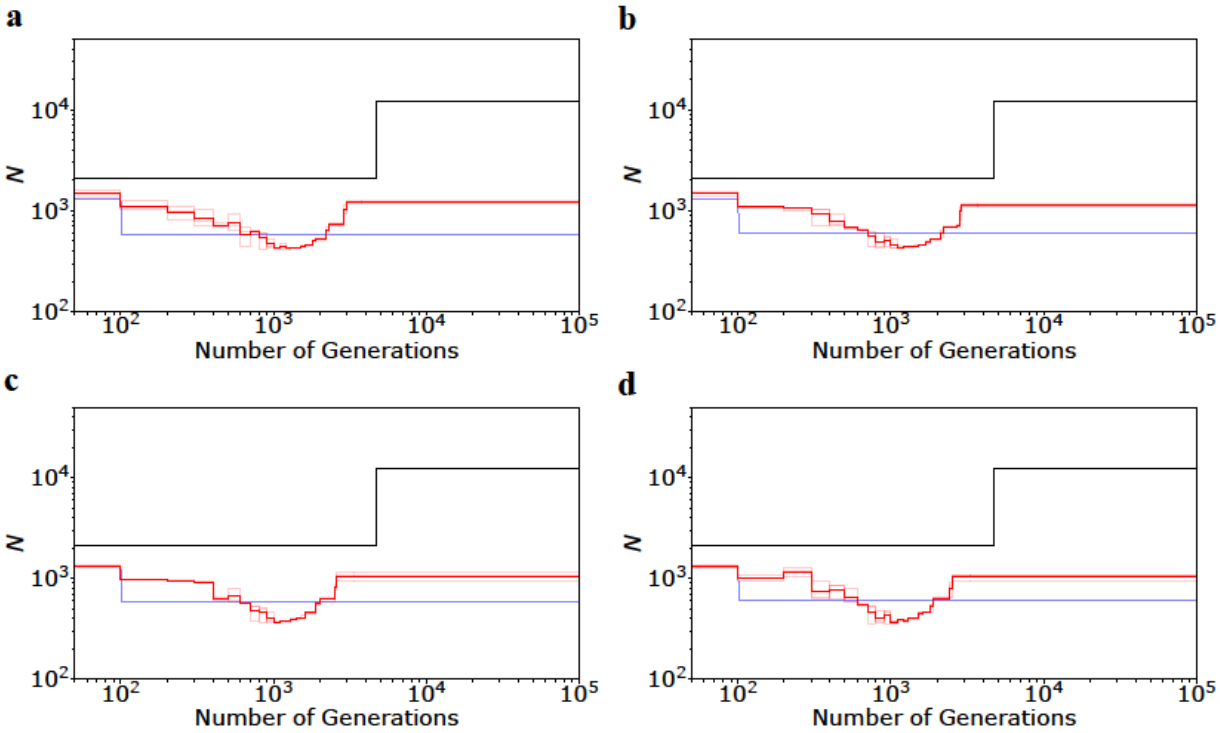

Supplementary Figure 11: Performance of demographic inference by MSMC (red lines) and *fastsimcoal2* (blue lines) in the presence of background selection, under different scenarios when the true model is a 6-fold instantaneous decline: (a) there is variation in recombination and mutation rates, (b) there is variation in recombination and mutation rates and the centromeric region is masked, (c) there is variation in recombination and mutation rates, and short regions resembling repeats (comprising 10% of each chromosome) are randomly masked across the genome, and (d) there is variation in recombination and mutation rates, and the centromere as well as small-sized repeats are randomly masked across the genome. Exons comprise of 20% of the genome, experience purifying selection given by DFE4 ($f_0 = f_1 = f_2 = f_3 = 0.25$), and are masked when performing inference.

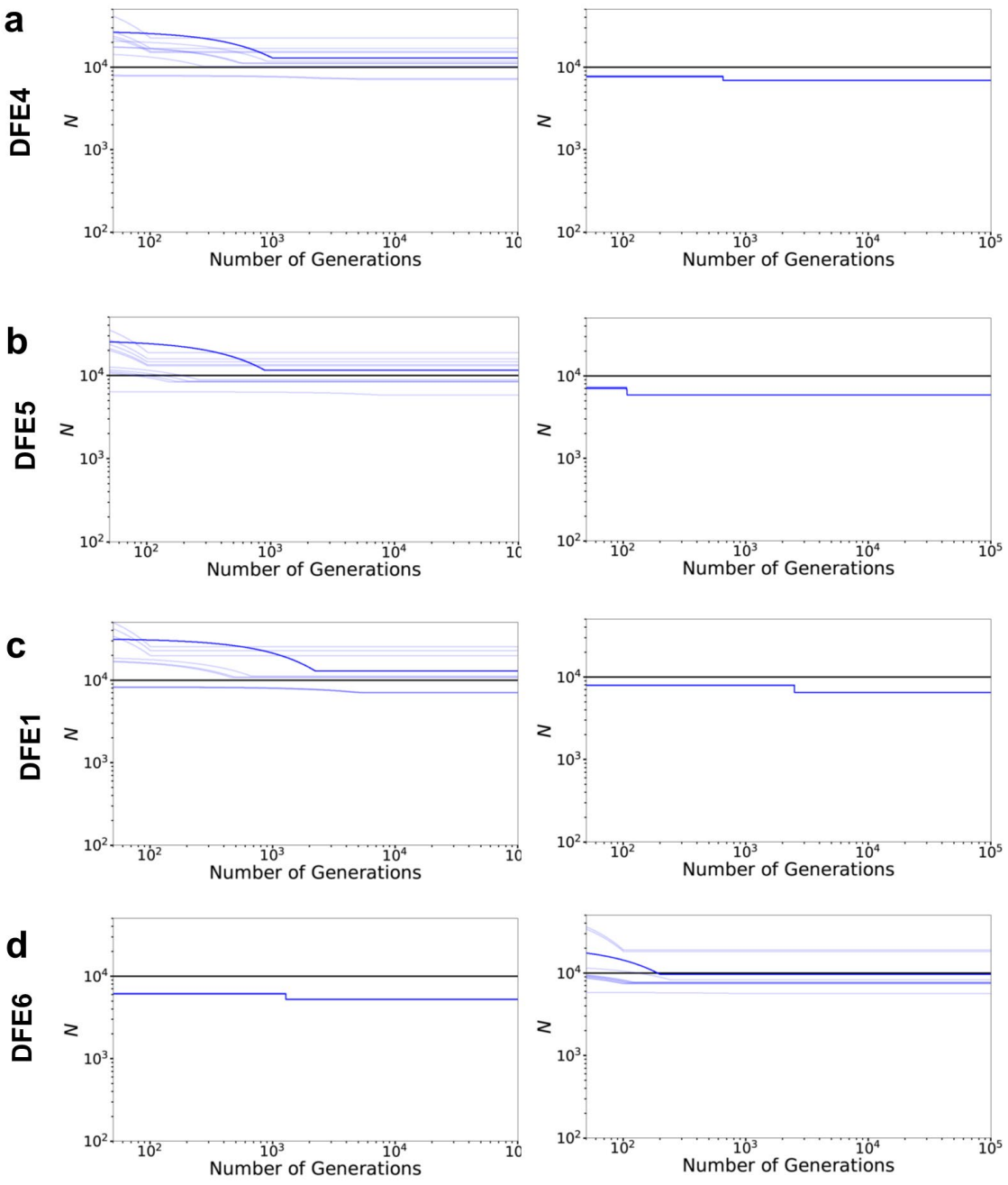

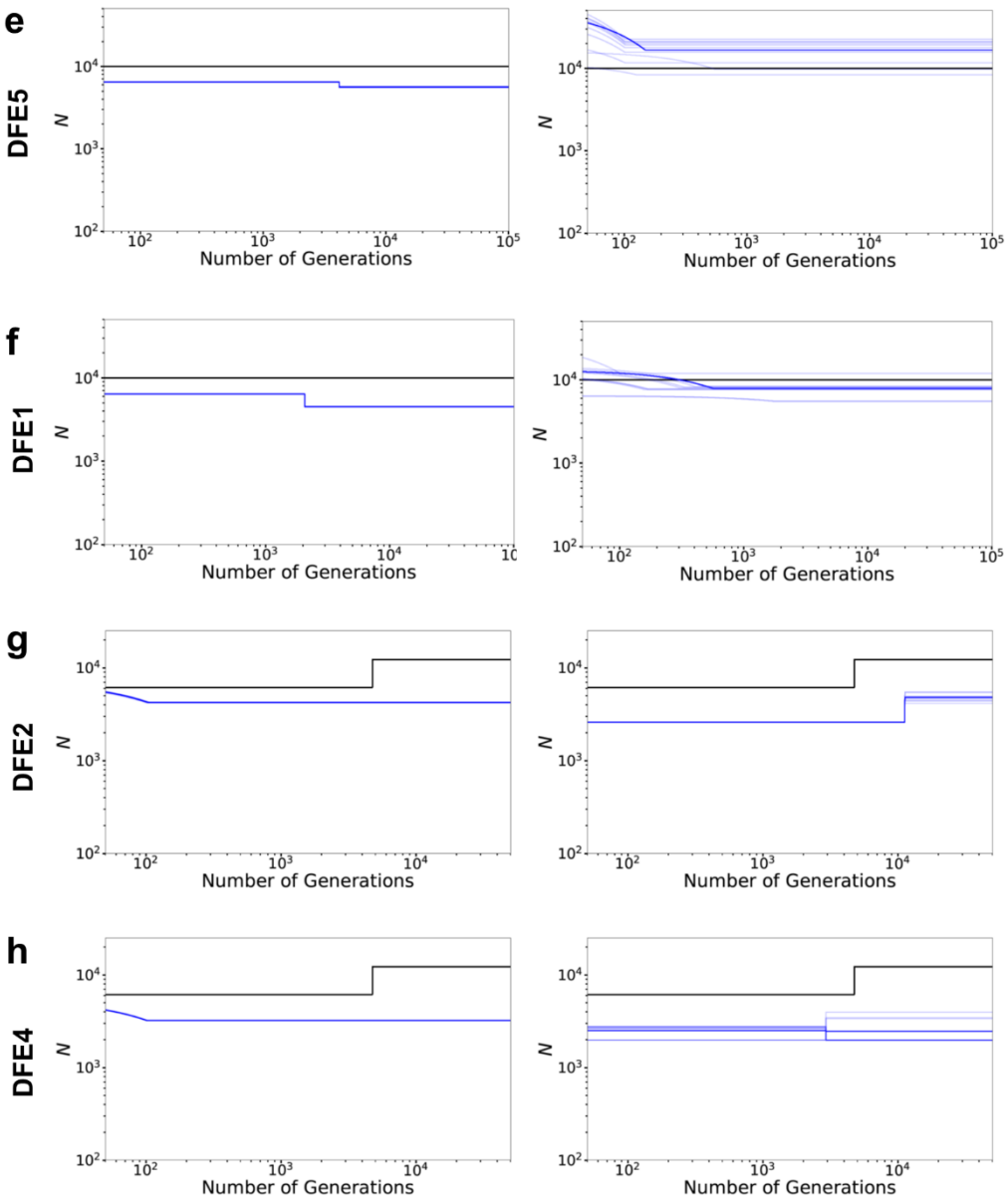

Supp Figure 12: Scenarios where demographic inference by *fastsimcoal2* resulted in different best models when performed using all SNPs (right column) and when SNPs were thinned to be separated by 5 kb (left column). The best model was defined as the model corresponding to the lowest AIC over all ten replicates. The DFEs are indicated on the left. (a) Direct purifying selection under DFE4 (exonic sites are not masked) in 5% of the genome; (b) Direct purifying selection under DFE5 (exonic sites are not masked) in 5% of the genome; (c) Direct purifying selection under DFE1 (exonic sites are not masked) in 10% of the genome; (d) Direct purifying selection under DFE6 (exonic sites are not masked) in 10% of the genome; (e) Background selection under DFE5 (*i.e.*, exonic sites are masked) in which 5% of the genome is exonic; (f) Background selection under DFE1 (*i.e.*, exonic sites are masked) in which 20% of the genome is exonic; (g) Background selection under DFE2 (*i.e.*, exonic sites are masked) in which 20% of the genome is exonic; (h) Background selection under DFE4 (*i.e.*, exonic sites are masked) in which 20% of the genome is exonic.

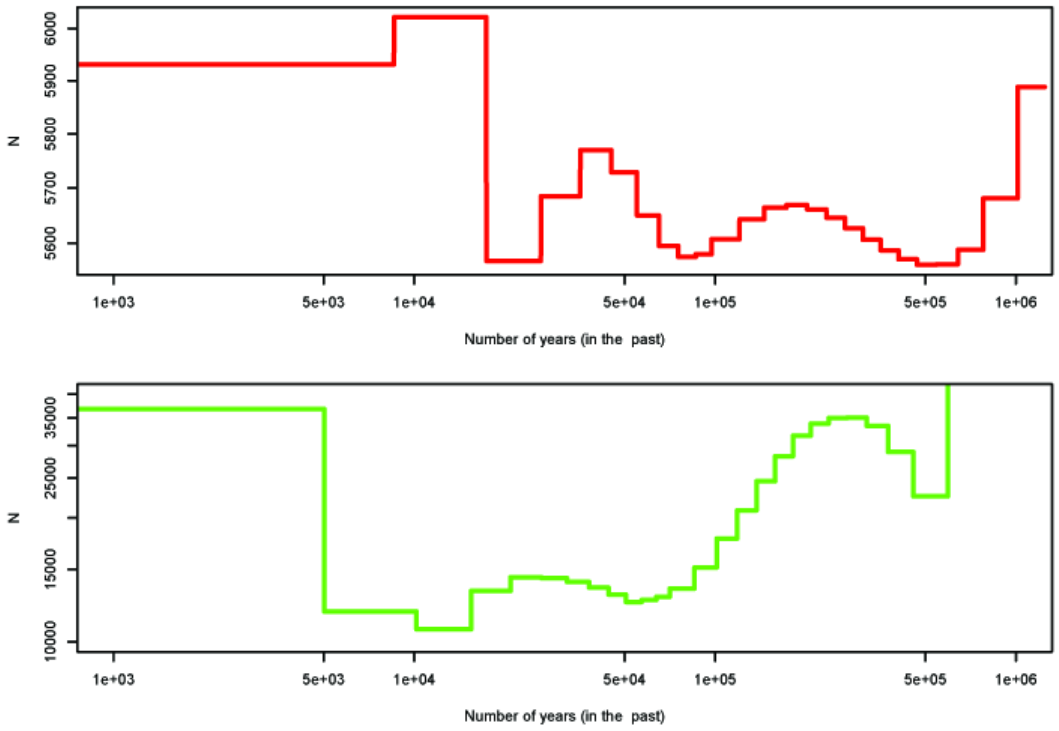

Supp Figure 13: Inference of demographic history by MSMC. Top panel / red line: simulations in which the true model is constant population size, and 50% of new mutations in exons are strongly deleterious with the remainder being neutral, where exons comprise 5% of the genome. Bottom panel / green line: the empirical estimate of population history of the YRI population inferred with MSMC by Schiffels and Durbin (2014). The x-axis is in years (assuming a generation time of 30 years). Note that the y-axes are on different scales, and the magnitude of change observed in the empirical data is considerably larger in the simulated data. Thus, this comparison is only meant to illustrate this common shape taken in MSMC plots (and see similar shapes in, for example, vervets (Warren *et al.* 2015; Figure 4) and passenger pigeons (Hung *et al.* 2014; Figure 2)).

Supp Table 1: Parameters underlying the human-like demographic models considered.

	Demographic models	**Ancestral population size**	**Current population size**	**Time of change in generations**
1	Equilibrium	10,000	10,000	NA
2	Exponential growth	1000	30,000	850
3	Instantaneous decline	12,300	2,100	4,750

Supp Table 2: Nucleotide diversity in the presence of BGS relative to that under neutrality (B) calculated for a neutral site distance y bases from the end of a gene/exon of length 500 bp. The exon experiences purifying selection with strength $2N_es=10$, where N_e is the effective population size and s is the reduction in fitness. Shown below is $t=hs$ where h is the dominance coefficient (assumed to be 0.5 here), r is the recombination rate per site per generation and u is the mutation rate per site per generation. B was calculated by using Equation 2 of Johri *et al*. (2020).

Ne	t ($2N_es$ =10)	r	u	B (y=1)	B (y=10)	B (y=1000)
10^4	0.00025	1.00×10^{-8}	1.00×10^{-8}	0.9805	0.9806	0.9820
		1.00×10^{-6}	1.00×10^{-6}	0.5152	0.5312	0.9444
10^6	2.5×10^{-6}	1.00×10^{-8}	1.00×10^{-8}	0.5152	0.5312	0.9445
		1.00×10^{-6}	1.00×10^{-6}	0.4920	0.8227	0.9992